Atmos. Chem. Phys., 17, 5035–5061, 2017
www.atmos-chem-phys.net/17/5035/2017/
doi:10.5194/acp-17-5035-2017

Atmospheric Chemistry and Physics Open Access EGU

Assessing the influence of NO_x concentrations and relative humidity on secondary organic aerosol yields from α-pinene photo-oxidation through smog chamber experiments and modelling calculations

Lisa Stirnweis[1,a], Claudia Marcolli[2,3], Josef Dommen[1], Peter Barmet[1,b], Carla Frege[1], Stephen M. Platt[1,c], Emily A. Bruns[1], Manuel Krapf[1], Jay G. Slowik[1], Robert Wolf[1], Andre S. H. Prévôt[1], Urs Baltensperger[1], and Imad El-Haddad[1]

[1]Laboratory of Atmospheric Chemistry, Paul Scherrer Institute, 5232 Villigen, Switzerland
[2]Institute for Atmospheric and Climate Science, ETH Zurich, 8092 Zurich, Switzerland
[3]Marcolli Chemistry and Physics Consulting GmbH, Zurich, Switzerland
[a]now at: Department of Radiation Protection and Environment, Federal Office for Radiation Protection, 85764 Oberschleissheim, Germany
[b]now at: Department Construction, Traffic and Environment, Canton of Aargau, 5001 Aarau, Switzerland
[c]now at: Department of Atmosphere and Climate, Norwegian Institute for Air Research, 2007 Kjeller, Norway

Correspondence to: Imad El-Haddad (imad.el-haddad@psi.ch) and Urs Baltensperger (urs.baltensperger@psi.ch)

Received: 9 August 2016 – Discussion started: 26 August 2016
Revised: 22 January 2017 – Accepted: 6 February 2017 – Published: 19 April 2017

Abstract. Secondary organic aerosol (SOA) yields from the photo-oxidation of α-pinene were investigated in smog chamber (SC) experiments at low (23–29 %) and high (60–69 %) relative humidity (RH), various NO_x / VOC ratios (0.04–3.8) and with different aerosol seed chemical compositions (acidic to neutralized sulfate-containing or hydrophobic organic). A combination of a scanning mobility particle sizer and an Aerodyne high-resolution time-of-flight aerosol mass spectrometer was used to determine SOA mass concentration and chemical composition. We used a Monte Carlo approach to parameterize smog chamber SOA yields as a function of the condensed phase absorptive mass, which includes the sum of OA and the corresponding bound liquid water content. High RH increased SOA yields by up to 6 times (1.5–6.4) compared to low RH. The yields at low NO_x / VOC ratios were in general higher compared to yields at high NO_x / VOC ratios. This NO_x dependence follows the same trend as seen in previous studies for α-pinene SOA.

A novel approach of data evaluation using volatility distributions derived from experimental data served as the basis for thermodynamic phase partitioning calculations of model mixtures in this study. These calculations predict liquid–liquid phase separation into organic-rich and electrolyte phases. At low NO_x conditions, equilibrium partitioning between the gas and liquid phases can explain most of the increase in SOA yields observed at high RH, when in addition to the α-pinene photo-oxidation products described in the literature, fragmentation products are added to the model mixtures. This increase is driven by both the increase in the absorptive mass and the solution non-ideality described by the compounds' activity coefficients. In contrast, at high NO_x, equilibrium partitioning alone could not explain the strong increase in the yields with RH. This suggests that other processes, e.g. reactive uptake of semi-volatile species into the liquid phase, may occur and be enhanced at higher RH, especially for compounds formed under high NO_x conditions, e.g. carbonyls.

1 Introduction

Organic aerosol (OA) accounts for 20–90 % of the submicron ambient aerosol (Jimenez et al., 2009, and references therein), a great part of which is secondary organic aerosol (SOA) formed via the condensation of oxidation products of gas-phase precursors. Several direct (e.g. radiocarbon dating)

and indirect observations underline the key role of biogenic volatile organic compounds (VOCs) for SOA formation (El Haddad et al., 2013, and references therein). Current state-of-the-art models are unable to predict the burden of biogenic SOA, especially in urban atmospheres (Hoyle et al., 2011), highlighting a fundamental deficit in our knowledge of the chemical pathways by which SOA accumulates and evolves in the atmosphere.

The ensemble of gaseous and particulate-phase species involved in SOA formation is immensely complex. The compounds relevant for SOA formation are often a minor fraction, resulting in yields (SOA formed to precursor reacted) of only a few percent. Their chemical composition and volatility distribution strongly depend on the oxidation conditions, most notably on the fate of organic peroxy radicals (RO_2), which react either with nitrogen oxides (NO_x) or other peroxy radicals (RO_2 and HO_2). The influence of NO_x on the oxidation mechanisms and SOA formation is commonly described by the NO_x / VOC ratio and has been under close scrutiny lately. For most light precursors, such as isoprene and monoterpenes (including α-pinene), SOA yields appear to be strongly influenced by the NO_x / VOC ratio, with a general enhancement observed under low NO_x conditions (Ng et al., 2007; Presto et al., 2005).

Species involved in SOA formation are subject to ongoing chemical degradation, which may lead to compounds of either lower (when functionalization dominates) or higher volatility (when fragmentation dominates). As a consequence, SOA yields and degrees of oxygenation (described by the atomic oxygen to carbon ratio O : C) may depend on the extent to which these species were exposed to oxidants (Kroll and Seinfeld, 2008; Donahue et al., 2012a).

SOA yields are generally described by the absorptive equilibrium partitioning of condensable species to a well-mixed liquid phase (Odum et al., 1996), which depends upon the chemical species' saturation vapour pressures (classically two model products are considered) and their liquid-phase activities (modified Raoult's law). Donahue and co-workers proposed the use of a "volatility basis set" (VBS) for a better representation of the wide range of OA in the atmosphere and the ongoing oxidation of semi-volatile organics (Donahue et al., 2011, 2012b, and references therein). However, several difficulties remain in estimating or measuring the saturation vapour pressures (e.g. Huisman et al., 2013; Bilde et al., 2015), activity coefficients and the mean molecular weight of the condensing species (e.g. Clegg et al., 2008a, b).

Difficulties increase when considering the role of relative humidity (RH) and of electrolyte particles in organic partitioning (Zuend and Seinfeld, 2013, and references therein). From a thermodynamic point of view, water interacts with SOA components by altering the water content of aerosol particles (also at subsaturated conditions) and hence the equilibrium concentration of water-soluble organic compounds. According to the equilibrium equation of Pankow (1994), an increase in the condensed fraction of the organics can be achieved by (1) increasing the absorptive particulate mass, (2) decreasing the average molecular weight of condensed species or (3) decreasing the activity coefficients of organic species. Therefore, it is expected that an increase in the particulate water content would in principle enhance SOA yields of water-miscible species. Model calculations predict a pronounced effect, especially at low organic mass loadings (Pankow, 2010). However, literature reports based on experimental results seem contradictory: RH-dependent yields have been reported for the ozonolysis of limonene, α-pinene and Δ^3-carene (Jonsson et al., 2006), while Prisle et al. (2010) found a negligible impact of RH on SOA yields from α-pinene ozonolysis. A substantial effect of RH on SOA yields was observed only for studies at precursor concentrations < 1000 ppbv and with large variation in RH (0.01 and 31 % RH (Bonn et al., 2002); < 2–58 % RH (Cocker et al., 2001); < 2–85 % RH (Jonsson et al., 2006).

The impact of RH on the partitioning of organic species may be severely suppressed by considerable deviations from ideal mixing between the condensing organic species and the prevailing condensed phase. A growing number of studies show that organic compounds are salted out in internally mixed organic/inorganic/water aerosol particles and two stable liquid phases may develop: an aqueous electrolyte solution and an organic solution (Marcolli and Krieger, 2006; You et al., 2014). The miscibility of an organic compound in aqueous droplets containing electrolytes depends on numerous factors, including temperature, relative humidity, organic compound polarity, the relative contribution of the compound to the bulk particulate matter and the chemical nature of the electrolytes (You et al., 2013; Zuend and Seinfeld, 2013). For example, phase separation was observed to always occur for organic compounds with O : C < 0.5 and at low relative humidity (You et al., 2013), and is especially pronounced in the case of ammonium sulfate (compared to ammonium hydrogen sulfate and nitrate). While neglecting phase separation of organic compounds and the effect of RH thereon bears the potential for invalid yield predictions (e.g. if the condensed phase is considered to comprise a mixed electrolyte and organic solution), the way the complex organic matrix interacts with water and the inorganic species remains virtually unknown.

Another complication that might influence the interpretation of chamber experiments conducted at different RHs is the enhancement of SOA yields by the potential reactive uptake of organic products into the particle phase (Kroll and Seinfeld, 2008; Kleindienst et al., 2006; Jang et al., 2002; Iinuma et al., 2007). The mechanisms by which such reactions occur are not fully identified, but may involve an ester or an aldol formation, which are expected to be favourable in the absence of water and are possibly catalytic under acidic conditions. Assessing the relative importance of particle-phase processing at different particle water contents would

require decoupling SOA thermodynamics and additional reactivity.

In this study, we examine the impact of particle water content on the chemical composition and yields of α-pinene SOA formed under low and high NO_x. This is performed by varying NO_x/α-pinene ratios, aerosol seed composition (hygroscopicity, acidity) and relative humidity. Results are parameterized within a thermodynamic framework to investigate whether changes in SOA non-ideal mixing properties with particle water content may explain the variation in SOA yields with RH. SOA yields reported here may aid the parameterization of the NO_x and particulate water dependence of α-pinene SOA production for further use in atmospheric models.

2 Methods

2.1 Experimental set-up and instrumentation

Twenty experiments, listed in Table 1, were carried out in the smog chamber (SC) of the Paul Scherrer Institute (PSI): a Teflon bag of 27 m^3 suspended in a temperature-controlled housing (Paulsen et al., 2005). Photochemistry was initiated by four xenon arc lamps (4 kW rated power, 1.55×10^5 lumens each, XBO 4000 W/HS, OSRAM), facing parallel to the SC bag, and emitting a light spectrum similar to the solar spectrum, and 80 black lights (Philips, Cleo performance 100 W) to accelerate the aging process, located underneath the SC bag, with emission between 300 and 400 nm wavelength (light characterization in Platt et al., 2013). A reflecting aluminium foil surrounds the SC bag to maintain light intensity and light diffusion.

Various parameters were monitored in the SC. The temperature (T) and RH measurement was optimized by passing SC air through a radiation shielded sensor. One of two different high-resolution time-of-flight aerosol mass spectrometers (HR-ToF-AMS, Aerodyne Research, Inc., Billerica, MA, USA) was operated during three different campaigns to measure the online size-resolved chemical composition (organics, ammonium, nitrate, sulfate, chloride) of non-refractory particles (DeCarlo et al., 2006). The HR-ToF-AMS were equipped with two different $PM_{2.5}$ lenses (Williams et al., 2013) to sample particles up to large diameters above 1 µm. The sampled aerosol was dried ($\sim$ 10 % RH) before measurement. A supporting flow of $\sim 1.5\,L\,min^{-1}$ was maintained parallel to the HR-ToF-AMS to minimize diffusive losses in the sampling lines.

The HR-ToF-AMS data were processed and analysed using the SQUIRREL (SeQUential Igor data RetRiEvaL) v.1.52L analysis software and PIKA (Peak Integration by Key Analysis) v.1.11L for the IGOR Pro software package (Wavemetrics, Inc., Portland, OR, USA). From the HR analysis of the mass spectra, the O : C ratios of the bulk OA were determined based on the parameterization proposed by Aiken et al. (2008). We note that while the assessment of the uncertainties related to the O : C measurements by the HR-ToF-AMS is not straightforward, a distinction should be made between measurement precision and accuracy. We do not expect the accuracy of the O : C ratios determined by the HR-ToF-AMS to be less than $\sim$ 20 % (Aiken et al., 2008; Pieber et al., 2016; Canagaratna et al., 2015; Bozzetti et al., 2017). For example, the use of a more recent parameterization (Canagaratna et al., 2015) would yield higher O : C values (by 18 %) and the O : C ratios reported here may be regarded as the lowest estimates. By contrast, relative changes in the O : C ratios are expected to be detected more precisely by the instrument ($\sim$ 1–2 %). The influence of potential biases and uncertainties in the determination of the O : C ratios on our results will be discussed in the text.

Two scanning mobility particle sizers (SMPS) were additionally deployed for the measurement of the aerosol size distributions. The first SMPS (a custom-built differential mobility analyser, DMA: extended length $L_{\mathrm{eff}} = 0.93$ cm, $d_{\mathrm{m\ max}} = 1000$ nm, recirculating sheath flow, and a condensation particle counter, CPC 3022 (TSI)) was connected to the HR-ToF-AMS sampling line to analyse the dried particles. A second SMPS ($SMPS_{wet}$, a TSI DMA classifier 3081 with recirculating sheath flow and a TSI CPC 3022A) and a CPC (TSI: CPC 3025A) measured the wet particle number size distribution and total number concentration ($d > 3$ nm), respectively.

Gas-phase compounds with a higher proton affinity than water (166.5 kcal mol^{-1}) were measured with a quadrupole proton transfer reaction mass spectrometer (PTR-MS, Ionicon). The PTR-MS was calibrated before each experiment for α-pinene, detected at m/z 137 and m/z 81; the accuracy of these measurements was estimated to be $\sim$ 5 %, based on the purity indicated on the calibration gas cylinder.

A modified NO_x instrument including a photolytic NO_2-to-NO converter (Thermo Environmental Instruments 42C trace level NO_x analyser equipped with a blue light converter) and two ozone monitors (Monitor Labs 8810 ozone analyser, Environics S300 ozone analyser) monitored NO_x and O_3 in the chamber.

2.2 Chamber operation and aerosol seeding

SOA formation and growth from α-pinene were induced by the following SC operation sequence: (1) humidification of the chamber, (2) addition of seed aerosol, (3) introduction of VOCs, (4) addition of nitrous acid (HONO) as an OH precursor, (5) addition of nitrogen oxides (equal amounts of $NO + NO_2$) if applicable, (6) an equilibration period (30–45 min), (7) switching on of xenon and black lights to generate OH radicals, and (8) a reaction time of 5 to 20 h (corresponding to 0–2×10^8 cm^{-3} h OH exposure; see Sect. 2.4). Experimental conditions for each individual experiment are summarized in Table 1. Prior to each experiment, cleaning of the SC was performed by the injection of several ppmv

Table 1. Overview of experimental conditions. Seed types (AHS: ammonium hydrogen sulfate (NH_4HSO_4); SA: sulfuric acid (H_2SO_4); AS: ammonium sulfate ($(NH_4)_2SO_4$); CF: fluorinated carbon (see Sect. 2.2)) and their assumed phase states: (L): liquid; (–): liquid and/or solid. Initial seed mass concentrations; relative humidity (RH); measured mean NO_x concentrations during low NO_x experiments (marked with an asterisk) and measured initial NO_x concentrations during high NO_x experiments; measured initial α-pinene concentrations (which reacted before an OH exposure of $(2.0 \pm 0.5) \times 10^7$ cm^{-3} h) and their estimated fractions reacted with OH radicals in %; the rest reacted with O_3). NO_x/α-pinene ratios; wall-loss-corrected organic mass concentrations (C_{OA}) and corresponding yields Y averaged over the OH exposure of $(2.0 \pm 0.5) \times 10^7$ cm^{-3} h. Standard deviations (1 SD) given in brackets are measurement variability. Horizontal lines separate experiments with different (i) seed composition, (ii) RH, and (iii) NO_x/α-pinene. Blank experiments (B1, B2 and B3) are listed at the very bottom.

No.	Seed		RH	NO_x	α-pin	α-pin decay	NO_x / α-pin	C_{OA} (wlc)	Yield, Y (wlc)
	type (phase)	initial		initial or mean(*)	initial = reacted	by OH		at OH exposure: $(2.0 \pm 0.5) \times 10^7$ cm^{-3} h	
		µg m^{-3}	%	ppbv	ppbv	%		µg m^{-3}	
1	AHS + SA (L)	8.0(0.5)	69(2)	44.4(0.8)	20.7	80.0	2.1	13.4(0.2)	0.115
2	AHS + SA (L)	12.3(0.5)	67(2)	70.4(1.3)	18.7	80.3	3.8	8.6(0.1)	0.081
3	AHS + SA (L)	4.9(0.3)	66(2)	19.6(0.7)	16.1	81.6	1.2	12.6(0.6)	0.138
4	AHS + SA (L)	4.7(0.2)	29(1)	23.6(0.6)	19.9	81.3	1.2	3.9(0.0)	0.035
5	AHS + SA (L)	8.0(0.3)	28(1)	52.1(0.6)	20.3	74.6	2.6	2.1(0.1)	0.018
6	AHS + SA (L)	5.2(0.3)	27(1)	1.3(0.4)*	18.3	87.8	0.071	12.0(0.5)	0.116
7	AS + AHS (L)	8.8(0.4)	67(1)	0.7(0.2)*	20.0	81.9	0.037	16.2(0.4)	0.143
8	AS + AHS (L)	4.3(0.6)	60(1)	1.0(0.2)*	18.7	86.5	0.052	12.3(0.4)	0.116
9	AS + AHS (L)	5.5(0.2)	56(2)	65.8(0.8)	30.9	65.0	2.1	11.1(0.1)	0.064
10	AS + AHS (L)	4.4(0.2)	50(1)	1.3(0.2)*	30.6	79.2	0.041	29.6(1.1)	0.171
11	AS + AHS (–)	4.1(0.2)	26(1)	0.7(0.3)*	18.9	81.3	0.039	5.5(0.2)	0.051
12	AS + AHS (–)	3.6(0.1)	26(1)	1.9(0.4)*	30.5	78.4	0.062	20.3(1.3)	0.118
13	AS + AHS (–)	8.2(0.3)	25(1)	1.1(0.3)*	19.6	87.4	0.055	5.3(0.1)	0.048
14	AS + AHS (–)	3.2(0.2)	23(1)	75.1(0.7)	27.8	69.4	2.7	2.4(0.1)	0.015
15	CF (L)	7.1(0.3)	58(1)	56.2(0.7)	31.7	67.9	1.8	9.8(0.1)	0.054
16	CF (L)	10.0(0.5)	58(2)	58.3(0.5)	31.3	73.9	1.9	10.7(0.1)	0.061
17	CF (L)	6.7(0.1)	26(1)	53.3(0.6)	30.5	69.7	1.7	4.7(0.1)	0.021
B1	CF (L)	0.3(0.1)	58(2)	53.0(0.6)	–	–	–	< 0.1	–
B2	AS + AHS (L)	4.5(0.7)	68(2)	0.9(0.5)*	–	–	–	2.8(1.0)	–
B3	AHS + SA (L)	3.8(0.2)	75(3)	1.4(0.3)*	–	–	–	0.5(0.1)	–

of ozone (5 h) and the simultaneous irradiation with black lights (10 h) at a temperature of 20 °C. This was followed by a pure air flushing period at high relative humidity (∼ 60 %) at a temperature of approximately 30 °C for at least 20 h. Three blank experiments (seed aerosol, lights switched on, high RH, but without adding α-pinene) were carried out to make sure that the organic aerosol formed during the experiments is not significantly influenced by background contamination in the SC. The organic mass concentration formed was substantially lower (< 0.1 up to 2.8 µg m^{-3}) than during comparable experiments (similar NO_x and RH).

In the chamber, the temperature varied between 21 °C and 26 °C. Due to heat from the xenon and black lights, the temperature increased, stabilizing only ∼ 1 h after experiment start. The increase in temperature of 1–4 °C led to an absolute decrease in RH of ∼ 2–20 %; thus, the RH range in Table 1, 23–67 %, is given for the stable temperature period. α-Pinene (98 %, Aldrich) and an OH reactivity tracer (9-times deuterated butanol, 98 %, D9, Cambridge Isotope Laboratories), hereafter referred to as butanol-d9 (1 µL injected ≈ 10 ppbv in the SC), were sequentially injected into an evaporation glass bulb heated to 80 °C. The two VOCs were transferred into the bag by a dilution and flush flow (each 15 L min^{-1}, maintained for 15 min) from an air purifier (737–250 series, AADCO Instruments, Inc., USA), further referred to as "pure air". Initial α-pinene concentrations were 16.1–31.7 ppbv.

HONO was used as a source of both NO and OH, produced by continuous mixing in a reaction vessel of the reagents sodium nitrite ($NaNO_2$, 1 mmol L^{-1} in milliQ-H_2O) and three different concentrations of sulfuric acid solutions (H_2SO_4, 1 mmol L^{-1} (experiments 1–6), 10 mmol L^{-1} (experiments 7, 8, 11, 13) and 100 mmol L^{-1} (experiments 9, 10, 12, 14) in milliQ-H_2O) (Taira and Kanda, 1990). HONO was carried by 2.5 ± 0.2 L min^{-1} pure air flow into the SC; 2 ppbv (± 10 %) of HONO were injected before lights on to initiate photochemistry and the injection was continued throughout all experiments. A chemiluminescence-based NO_x instrument (Monitor Labs 9841A NO_x analyser) was attached to the HONO source to monitor the injected concentration throughout the experiment. In addition, equal concentrations of NO (99.8 %; 1005 ppmv $\pm$ 2 %) and NO_2 (purity: 98 %; 1005 ppmv $\pm$ 3 %), resulting in 19.6–75.1 ppbv initial NO_x, were added during experiments with NO_x/α-pinene > 1. Within the results section, the two terms "low NO_x" and "high NO_x" refer to the following conditions.

- Low $NO_x = NO_x/\alpha$-pinene < 0.1, with continuous HONO injection, indicated by an asterisk in Table 1 and figures.
- High $NO_x = NO_x/\alpha$-pinene > 1: initial injection of $NO + NO_2$ with continuous HONO injection.

In Table 1, we report for high NO_x conditions the initial NO_x concentration (which decays with time), and for low NO_x conditions the mean NO_x concentration. We note that the NO levels are the main driver in determining whether RO_2–NO or RO_2–RO_2 reactions would prevail. Based on our calculations (not shown here; see Platt et al., 2014), RO_2 radicals would predominantly react with NO, when the concentration of the latter is higher than only 1 ppbv. These conditions can be considered high NO_x. During high NO_x experiments and throughout the period when the majority of α-pinene was consumed, the NO concentration remained higher than 5 ppbv, indicating that α-pinene oxidation proceeded under high NO_x. During low NO_x experiments, the average NO_x concentration was around 1–2 ppbv, predominated by NO_2, while the NO concentrations were below detection limits (< 0.1 ppbv). Under these conditions RO_2–RO_2 reactions may prevail.

During 14 experiments (nos. 1–14) and 3 blank experiments, an ammonium hydrogen sulfate (NH_4HSO_4, Aldrich) solution in ultrapure Milli-Q water (1 g L^{-1}) was nebulized (0.6 L min^{-1}) and introduced into the SC with a pure air dilution flow of 10 L min^{-1} to act as seed particles. To keep the seed aerosol in a liquid state, no drier was used behind the nebulizer. We determined the acidity of the seed particles, here described by the ratio NH_4 / SO_4, by the comparison between the HR-ToF-AMS measurements of the seed particles and nebulized $(NH_4)_2SO_4$ and NH_4HSO_4 solutions. An NH_4 / SO_4 ratio between 1 and 2 indicates a rather neutral seed composition, representing a mixture of NH_4HSO_4, $(NH_4)_3(SO_4)_2$ (letovicite) and $(NH_4)_2SO_4$. For simplicity, we replaced $(NH_4)_3(SO_4)_2$ with an equal mix of NH_4HSO_4 and $(NH_4)_2SO_4$ for the assumption of density and growth factors. By contrast, NH_4 / $SO_4 \leq 1$ indicates an acidic seed, consisting of NH_4HSO_4 and H_2SO_4.

During experiments 7–14, the nebulized NH_4HSO_4 solution was partly neutralized to $(NH_4)_2SO_4$, presumably by background NH_3 (Fig. S1 in the Supplement). During experiments 1–6 the seed was composed of an aqueous mixture of NH_4HSO_4 and H_2SO_4, due to the in situ production of gas-phase H_2SO_4 via the HONO injection system, suppressing the seed neutralization by NH_3 (even though particulate H_2SO_4 was minimized by a Teflon filter applied between the HONO source and the SC).

Additionally, three α-pinene experiments (nos. 15–17) and one blank experiment were conducted using an inert hydrophobic fluorinated hydrocarbon seed (further referred to as the CF seed; $CF_3CF_2CF_2O$–[$CF(CF_3)CF_2$–O–]$_n CF_2CF_3$; Krytox® 1525). The CF seed was generated via the evaporation of the pure compound at a temperature of 125–145 °C and subsequent homogeneous nucleation in a pure air flow of 2.4 ± 0.1 L min^{-1}. The CF-seed concentration was 6.7–10 µg m^{-3} when lights were switched on, and decayed very rapidly to values below the detection limit of the HR-ToF-AMS (0.1 µg m^{-3}) during the course of the experiment. The CF-seed mass spectrum in the HR-ToF-AMS is clearly distinct from that of α-pinene SOA, with main contributions at m/z 69 (CF_3), m/z 169 (C_3F_7) and m/z 119 (C_2F_5) (Fig. S2 and Table S1 in the Supplement).

Table 1 lists the expected physical state and seed composition of each experiment dependent on RH (AHS: ammonium hydrogen sulfate (NH_4HSO_4); AS: ammonium sulfate ($(NH_4)_2SO_4$); SA: sulfuric acid (H_2SO_4); CF: fluorinated carbon). Submicrometer AS particles and letovicite particles ($(NH_4)_3H(SO_4)_2$) are expected to effloresce at about 35 % RH, while more acidic particles should remain liquid between 20 and 30 % RH (Martin, 2000; Ciobanu et al., 2010).

2.3 Estimation of the hygroscopic growth factors and liquid water content

The absolute liquid water content (LWC) of the aerosol particles was derived for the bulk aerosol mass and the size-resolved mass distribution, based on literature growth factors, the measured RH and chemical composition. The growth factor GF (RH) of a particle is defined as the ratio of the wet diameter at a given RH to the dry diameter: $GF(RH) = d(RH)/d_{dry}$. Inorganic GFs were taken from the Aerosol Diameter Dependent Equilibrium Model (ADDEM, Topping et al., 2005) for diameters of 360 nm. Organic GFs were derived using the relationship between the hygroscopicity parameter κ and the degree of oxygenation [$\kappa = 0.29 \times (O:C)$] from Chang et al. (2010), well representing the hygroscopicity of α-pinene SOA measured by Massoli et al. (2010). The measured degree of oxygenation at an

OH exposure of $(2.0 \pm 0.5) \times 10^7$ cm^{-3} h was used to derive κ, which in turn was converted to GF, assuming a negligible curvature (Kelvin) effect (Kreidenweis et al., 2005):

$$\mathrm{GF(RH)} = \left(1 + \kappa \frac{\frac{\mathrm{RH}}{100\,\%}}{1 - \frac{\mathrm{RH}}{100\,\%}}\right)^{\frac{1}{3}}. \quad (1)$$

The mixed GFs for aerosol containing inorganic and organic species were determined using as a first approximation the Zdanovskii–Stokes–Robinson (ZSR) volume mixing rule (Stokes and Robinson, 1966):

$$\mathrm{GF_{mixed}\,(RH)} = \left(\sum_i \varepsilon_i \times (\mathrm{GF}_i\,(\mathrm{RH}))^3\right)^{\frac{1}{3}}, \quad (2)$$

where ε_i and GF_i(RH) denote the volume fraction and GF (RH) of species i, respectively. The H_2O volume (V_{H_2O}) was calculated using the definition of GF (RH) and the dry volume (V_{dry}):

$$V_{H_2O} = V_{dry} \times \left(\mathrm{GF(RH)}^3 - 1\right). \quad (3)$$

V_{H_2O} multiplied by the density of water (1 g cm^{-3}) results in the LWC.

The dry (S_{dry}) and wet (S_{wet}) surfaces from HR-ToF-AMS size-resolved data were calculated with Eqs. (4) and (5), respectively:

$$S_{dry} = 6 \times (V_{dry})/d_{dry}, \quad (4)$$

$$S_{wet} = 6 \times (V_{dry} + V_{H_2O})/(\mathrm{d\,(RH)}). \quad (5)$$

The LWC and surface distributions were calculated using size-resolved pToF (particle time-of-flight) data of the HR-ToF-AMS. Due to the low pToF signal of NH_4, the NH_4 surface distributions were estimated based on SO_4 pToF measurements.

2.4 Determination of OH exposure and extent of α-pinene ozonolysis

The gas-phase composition, the OH concentration and the photochemical age of a chemical reaction system may considerably differ between experiments of the same duration. Furthermore, variation of the OH concentration within a single experiment means that the photochemical age is not necessarily directly proportional to the light exposure time. Consequently, we discuss reaction time in terms of OH exposure (mol cm^{-3} h), defined as the OH concentration integrated over time. OH exposures were derived based on the decay of the OH tracer butanol-d9, detected by the PTR-MS as $M + H^+$–H_2O at m/z 66, following the methodology introduced by Barmet et al. (2012). The OH exposure was determined by the integration of the following expression:

$$\mathrm{OHexposure} = -\int_{t_1=0}^{t} \left(\frac{1}{k_{\mathrm{OH,butanol-d9}}} \times \left(\frac{\Delta \ln(\mathrm{butanol-d9})}{\Delta t} + \frac{f_{\mathrm{dil}}}{V}\right)\right) \mathrm{d}t, \quad (6)$$

where butanol-d9 and $k_{\mathrm{OH,\,butanol-d9}}$ ($= 3.4 \times 10^{-12}$ cm^3 mol^{-1} s^{-1}) are the butanol-d9 concentration and its reaction rate constant against OH, respectively, t is the time after lights on, V the chamber volume (we assume as a first approximation a constant chamber volume of 27 m^3), and f_{dil} the dilution flow due to HONO input (Sect. 2.2).

The percentage of α-pinene reacted with OH and O_3 was derived based on Eq. (7):

$$-\frac{\mathrm{d}(\alpha - \mathrm{pin})}{\mathrm{d}t} = k_{\mathrm{O_3},\alpha-\mathrm{pin}}\,[\mathrm{O_3}] \times [\alpha - \mathrm{pin}] + k_{\mathrm{OH},\alpha-\mathrm{pin}}\,[\mathrm{OH}] \times [\alpha - \mathrm{pin}] + \frac{f_{\mathrm{dil}}}{V}, \quad (7)$$

where [α-pin], [O_3] and [OH] denote the concentrations of α-pinene (measured by the PTR-MS at m/z 137 and 81), O_3 and OH, respectively, and $k_{\mathrm{OH},\,\alpha\text{-pin}}$ ($= 5.3 \times 10^{-11}$ cm^3 mol^{-1} s^{-1}) and $k_{\mathrm{O_3},\,\alpha\text{-pin}}$ ($= 8.9 \times 10^{-17}$ cm^3 mol^{-1} s^{-1}) the reaction rate constants of α-pinene with OH and O_3, respectively. The percentage of α-pinene reacted with OH is presented in Table 1 and discussed in Sect. 3.4.

2.5 Determination of suspended and wall-loss-corrected organic masses and yields

Suspended OA mass. The suspended organic mass concentration $C_{\mathrm{OA}}^{\mathrm{sus}}$ was derived by utilizing the chemical composition measurements from the HR-ToF-AMS scaled to the total volume measured by the SMPS (Figs. S3 and S4), using compound-specific densities ($\rho_{\mathrm{org}} = 1.4$ g cm^{-3}, $\rho_{NH_4HSO_4} = 1.79$ g cm^{-3}, $\rho_{(NH_4)_2SO_4} = 1.77$ g cm^{-3}, $\rho_{H_2SO_4} = 1.83$ g cm^{-3}).

For some experiments (9, 10, 12 and 14–17), the organic mass concentrations determined by the HR-ToF-AMS were corrected for a sub-unity transmission efficiency at the lower edge cut-off of one of the two $PM_{2.5}$ lenses employed (Figs. S3 and S4). Additionally, for organic mass calculation, we assumed that the measured NO_3 signals are entirely related to organonitrates ($RONO_2$), rather than NH_4NO_3. This assumption mainly stems from (1) the observation of the NO_3 signal in the same particle size region as OA rather than SO_4^{2-} (see the size-resolved pToF data, Sect. 3.3), while inorganic nitrate would be expected to mix within an electrolyte-rich aerosol and (2) the presence of NO_3 under acidic conditions, which are thermodynamically unfavourable for the partitioning of nitric acid. This is also supported by the higher

NO^+ / NO_2^+ ratios measured in the SC compared to ratios recorded during NH_4NO_3 nebulization (on average 1–2.8 times higher, Fig. S5), typically expected from organonitrates (Farmer et al., 2010). We cannot exclude a part of the NO_3 signal originating from NH_4NO_3. However, even attributing all detected nitrate to NH_4NO_3 would increase the calculated LWC by 1–13 % and decrease the calculated OA mass by 2–7 % only, which would not influence our conclusions. Finally, for yield calculations we assume the accuracy of the aerosol-phase measurements to be 30 % (Canagaratna et al., 2007).

Wall-loss-corrected OA mass. To obtain the total C_{OA} concentration corrected for losses of particles and vapours to the chamber walls, we use Eq. (8), introduced by Hildebrandt et al. (2011), based on the mass balances of the suspended organic aerosol mass, C_{OA}^{sus}, and the mass of the organic aerosols on the walls, C_{OA}^{walls} (summed up to derive C_{OA}).

$$\frac{d}{dt}\left[C_{OA}^{walls}(t)\right] = k_{OA}^{w}(t)\, C_{OA}^{sus}(t) + \omega(t) \times \left(k_{OA}^{w}(t)\, C_{OA}^{sus}(t) + \frac{d}{dt}\left[C_{OA}^{sus}(t)\right]\right) \times \frac{C_{OA}^{walls}(t)}{C_{OA}^{sus}(t)} \quad (8)$$

Here, k_{OA}^{w} represents the loss rate constant of organic particles to the walls, derived by fitting the suspended organic mass concentration 5–8 h after lights were switched on in the SC, when SOA production is expected to be negligible (α-pinene concentration < 1 ppbv, Fig. S6 and Table S2). We determine an average loss rate of $0.13\,\mu g\,m^{-3}\,h^{-1}$, corresponding to a particle half-life of 5.3 h. The average k_{OA}^{w} was used in the case of insufficient statistics to perform accurate fitting. In Eq. (8), ω, ranging between 0 and 1, is a dimensionless proportionality coefficient between the mass of organic vapours that partition onto the wall-deposited particles and the mass of organic vapours that partition onto the suspended particles. Here, we neglect the condensation of organic vapours onto the wall-deposited particles, i.e. $\omega = 0$, consistent with previous studies of α-pinene SOA production (Hildebrandt et al., 2011, and references therein). This assumption gives a lowest estimate of SOA yields, but does not influence the comparison between the experiments. Considering the second limiting case $\omega = 1$, i.e. an equal partitioning of organic vapours between the wall-deposited and suspended particles, would increase the determined SOA yields (by up to 40 %, and by 20 % on average).

Equation (8) does not take into consideration the loss of SOA-forming vapours onto the clean Teflon walls, which may suppress SOA yields from laboratory chambers under certain conditions. These processes may be related to the vapours' reactive uptake onto walls (Loza et al., 2010; Nguyen et al., 2016) or to their absorptive uptake (Zhang et al., 2014; Nah et al., 2016). The reactive uptake of organic vapours onto chamber walls is only significant at high RH. Loss rates for important reactive gases, including glyoxal, epoxides and peroxides, have been documented at different RHs (Loza et al., 2010; Nguyen et al., 2016). While these processes may also influence reactive SOA-forming compounds under our conditions, they occur at timescales of hours (Nguyen et al., 2016), much longer compared to the timescales of the absorptive uptake, e.g. based on recent direct measurements of vapour losses onto Teflon walls ($\sim$ 10 min, Krechmer et al., 2016).

The absorption of organic compounds into the chamber walls obeys Henry's law and depends on the compounds' accommodation coefficients and their activity at the wall–gas interface (see for example Zhang et al., 2015). The dependence of the compounds' absorption on RH (due to a change in accommodation coefficients or in the activity of the wall-absorbed compounds) has not yet been reported to the best of our knowledge and indeed merits further investigations that are beyond the scope of the current study. Nevertheless, we believe that vapour absorption onto the walls is unlikely to be significantly affected by RH, due to the hydrophobic nature of Teflon and its minor interaction with water under subsaturation conditions (RH < 80 %). In our case, we have maintained chamber conditions during our experiments such that vapour wall losses and their inter-experimental differences can be minimized as much as possible. This is done by (1) maintaining a relatively constant wall-to-seed surface ratio for all experiments to avoid systematic biases between experiments and (2) increasing SOA production rates, which rapidly provide a significant particle condensational sink into which condensable gases can partition. We also note that vapour wall losses were found to be minor for the α-pinene SOA system, where SOA formation is dominated by quasi-equilibrium growth (Zhang et al., 2014; Nah et al., 2016).

SOA yields determination and parameterization. SOA mass yields, Y (dimensionless quantity), are calculated from Eq. (9), as the organic mass concentration formed, C_{OA}, per precursor mass consumed, $\Delta C_{\alpha\text{-pinene}}$:

$$Y = \frac{C_{OA}}{\Delta C_{\alpha\text{-pinene}}}. \quad (9)$$

For comparison purposes, Y values are reported in Fig. 2 and Table 1 and discussed in Sect. 3 at an OH exposure of $(2.0 \pm 0.5) \times 10^7\,cm^{-3}\,h$, reached during all experiments. The parameterization of smog chamber SOA yields measured is based on the absorptive partitioning theory of Pankow (Eq. 10), which expresses the production of a set of semi-volatile surrogate products (total number N) as a function of the mass yield of these products, α_i, and their partitioning coefficients, ξ_i (a dimensionless quantity reflecting the condensed-phase mass fraction of these products). The critical parameters driving the partitioning of these products are their effective saturation concentration, C_i^*, and the total concentration of the absorptive organic phase, C_{OA}. As discussed below, we consider the absorptive organic mass as the sum of the total OA concentration and the liquid water in this

phase (Sect. 3.3).

$$Y = \sum_{i}^{N} \alpha_i \xi_i = \sum_{i}^{N} \alpha_i \left(1 + \frac{C_i^*}{C_{\mathrm{OA}}}\right)^{-1} \quad (10)$$

In Eq. (10), C_i^* (in $\mu g\,m^{-3}$) is a semi-empirical property (inverse of the Pankow-type partitioning coefficient, $K_{\mathrm{P},i}$) reflecting the saturation vapour pressure of the pure constituents $\left(p^{\mathrm{o}}_{\mathrm{L},i}\right)$ and the way they interact with the organic mixture (effectively including liquid-phase activity coefficients, γ_i), as expressed in Eq. (11):

$$C_i^* = \frac{10^6 M_i \gamma_i p^0_{\mathrm{L},i}}{760\ \mathrm{RT}}. \quad (11)$$

Here, M_i denotes the compound molecular weight, R the ideal gas constant and T the temperature. Smog chamber yields from single experiments are fitted as a function of C_{OA} using the volatility basis set (VBS) (Donahue et al., 2006), which separates semi-volatile organics into logarithmically spaced bins of effective saturation concentrations C_i^*. Figure 5 shows the resulting parameterizations (lines) in comparison to the measured data (symbols) for each experiment.

To determine the yields per volatility bin (α_i), wall-loss-corrected SOA yields, Y as a function of wall-loss-corrected absorptive mass concentration C_{OA} (data presented in Fig. 5), were used. We assumed a total number of five bins: $N = 5$ with $C_i^* = 0.01$, 0.1, 1, 10 and $100\,\mu g\,m^{-3}$. To solve Eq. (10) for the parameters α_i, we introduced a novel approach using a Monte Carlo simulation. This approach provides best estimates of α_i values (data shown in Figs. 6 and S7), together with a measure for the uncertainties related to the determination of the volatility distributions from SC experiments. The calculation proceeded as follows.

1. From the calculated yields (Y), lower (Y_1) and upper (Y_2) yield curves were determined based on the estimated measurement accuracy of C_{OA} and α-pinene mass. A possible yield domain was inscribed against C_{OA} by plotting Y_1 and Y_2 versus their corresponding lower and upper C_{OA}, respectively. The parameterized yield curves are shown in Fig. 5.

2. A range of possible inputs was defined for each of the parameters α_i. This range is restricted within the following interval: $[0; 2 \times (Y_i - Y_{i-1})]$. This step was only necessary for computational reasons.

3. α_i parameters were randomly generated over the defined intervals.

4. Deterministic computations of Y versus C_{OA} were performed using Eq. (10) and the generated α_i inputs.

5. Volatility distributions that fell within the domain defined in step (1) were retained, aggregated and presented as probability distribution functions for each of the five effective saturation concentrations C_i^* (probability density function, PDF, Figs. 6 and S7).

2.6 Thermodynamic modelling

General principles. Using thermodynamic modelling, we seek to understand whether observed changes in SOA bulk properties (yields and O : C ratios) with RH can be explained by a change in the particles' thermodynamic properties. Gas–liquid and liquid–liquid phase partitioning calculations are performed following the methods developed in Zuend et al. (2008, 2010, 2012) and Zuend and Seinfeld (2013), using the thermodynamic group-contribution model, AIOMFAC (Aerosol Inorganic-Organic Mixtures Functional groups Activity Coefficients), to calculate activity coefficients. This approach enables prediction of the phase partitioning of known organic compounds knowing their abundances in a given known mixture of organic species and electrolytes at a given RH and temperature.

The modelling requires the use of explicit surrogate compounds. Based on Eq. (10), the partitioning of these compounds is driven by their volatility distributions, which depends on (1) the compounds' effective saturation concentrations and (2) their relative abundances. Compounds' effective saturation concentrations, used as model inputs, were calculated based on Eq. (11) initially assuming ideal mixing ($\gamma = 1$) and utilizing vapour pressures estimated using EVAPORATION (Compernolle et al., 2011). The relative abundances of these compounds in the model mixtures are based on the volatility distributions derived from experimental data (Sect. 2.5).

We assumed instantaneous reversible absorptive equilibrium of semi-volatile organic species into ideal and non-ideal liquid-phase aerosols. In the case of non-ideal solutions, positive and negative deviations of mole fraction-based activity coefficients from unity indicate the degree of non-ideality in a mixture. The activity coefficients take into account the compounds' affinity towards the solution (interactions with other organic species, electrolytes and water) and hence depend on the solution's chemical composition. Therefore, the activity coefficients for the different organic species cannot be set a priori, but are calculated iteratively in the model, until convergence of the compounds' abundances in the different phases; see (Zuend et al., 2008, 2011).

We considered cases with and without interactions between the electrolyte and organic phases, which enables one to assess the solubility of the organic compounds in the inorganic seed aerosols. Seed concentrations in $\mu g\,m^{-3}$ were transformed into moles of seed per volume ($mol\,m^{-3}$) assuming equal shares of AHS and SA for acidic seeds and equal shares of AHS and AS for neutral seeds. Because interaction parameters of some organic functional groups with HSO_4^- are missing in AIOMFAC, we assumed the interactions of organic compounds with HSO_4^- and with SO_4^{2-} to be similar. For all computations, metastable supersaturated salt solutions were allowed.

Model compounds are only surrogates. The choice of these surrogates should reflect the wide range of volatility and hy-

drophilicity of SOA species. We have selected as surrogates α-pinene photo-oxidation products reported in the literature, identified under different NO_x and aerosol seed conditions, covering the wide range of volatility relevant to SOA. Compound hydrophilicity instead depends heavily on the number of functional groups present in the molecule, which can be largely simulated by the compound O : C ratio (Zuend and Seinfeld, 2012). As increasing the compound O : C ratio also decreases its volatility, we have considered cases with and without fragmentation products with a shorter carbon backbone chain but high O : C ratios, expected to be representative of later-generation photolysis and photo-oxidation products (Mutzel et al., 2015; Krapf et al., 2016). This approach would effectively decouple compounds' hydrophilicity and volatility and allow scanning of both properties independently. While we recognize that oxidation conditions, e.g. NO_x concentrations, may significantly alter the product distribution, we did not select different sets of products for the different conditions. This is because

1. such a separation would implicitly suggest that the chemical composition of the few compounds reported at different conditions can be extrapolated to the bulk OA under our conditions;
2. such a separation would significantly limit the number of surrogates at each condition, increasing the sensitivity of the model to the compounds' selection; and
3. the model is less sensitive to the compounds' chemical structure than to their elemental composition (see below and Li et al., 2016), e.g. number of oxygen and carbon, which has been taken into account by including fragmentation products.

The relative abundance of the selected compounds is optimized in the model for each experiment at the prevailing RH such that the modelled and measured SOA yield and O : C ratio match. Then, the RH is modified in the model, and changes in the SOA yields and O : C ratios are compared to the observations. Model calculations were performed at an OH exposure of $(2.0 \pm 0.5) \times 10^7$ cm^{-3} h. In the following we thoroughly describe the different steps involved in the model setting.

Simulated cases. The following simulations were performed.

1. Case org: non-ideal partitioning, including liquid–liquid phase separation (LLPS; activity coefficients calculated with AIOMFAC), of the organic compounds between the gas phase and a purely organic aerosol phase neglecting the presence of the seed aerosol and using reported model compounds only;
2. Case id: ideal partitioning (activity coefficients all set to unity; LLPS cannot occur) between gas phase and organic aerosol phase using reported model compounds only;
3. Case sd: non-ideal partitioning including the seed aerosol to an internally mixed organic/AS aerosol using reported model compounds only;
4. Case sdfr: non-ideal partitioning including the seed aerosol to an internally mixed organic/AS aerosol including the formation of fragmented oxidation products (see below);
5. Case orgfr: non-ideal partitioning including LLPS to a purely organic aerosol phase neglecting the presence of the seed, including the formation of fragmented oxidation products.

α_i parameters determined through the Monte Carlo simulations assume that the absorptive mass consists of the organic phase (in accordance with assumptions in chemical transport models). This assumption is violated for cases sd and sdfr as compounds may partition into the inorganic phase. Nevertheless, the results obtained for these cases may still be examined in relative terms to inspect the effect of RH on SOA yields in the presence of an inorganic seed and the partitioning of SOA compounds between the inorganic and organic phases.

Model compounds. To simulate SOA partitioning in AIOMFAC, α-pinene photo-oxidation products reported in the literature (Eddingsaas et al., 2012; Jaoui and Kamens, 2001; Kleindienst et al., 2007; Valorso et al., 2011) were chosen as model compounds for cases org, id and sd, namely ValT4N10 (10th compound in Table 4 from Valorso et al., 2011), 3-hydroxyglutaric acid, pinic acid, hopinonic acid, norpinic acid, 2-hydroxyterpenylic acid, 10-oxopinonic acid, and 4-oxopinonic acid. These compounds are listed in Table S4 together with their relevant physicochemical properties (MW, O : C ratio, vapour pressures and chemical structures). For cases sdfr and orgfr, additional oxidized fragmented products (3-oxoadipic acid, glutaric acid, 5-COOH-3-OH-pentanal, and succinic acid) were included (Table S4). While these compounds were not reported to derive from α-pinene oxidation, their structure, including carbon and oxygen numbers, is very similar to the most abundant compounds detected by Chhabra et al. (2015) and Mutzel et al. (2015) using chemical ionization mass spectrometry. Volatility distributions could reliably be determined for volatility bins $C^* = 0.1$–$100\,\mu g\,m^{-3}$. Nevertheless, lower volatility products with $C^* = 0.01\,\mu g\,m^{-3}$ are also formed. Therefore, this bin was loaded for all phase partitioning calculations with equal fractions of the model compounds diaterpenylic acid acetate, 3-MBTCA and ValT4N9 with mass yields of 10^{-5} each. This low mass fraction does not influence the organic yield, but proved to aid the convergence of the phase partitioning calculation. To achieve mass closure in the model, pinonaldehyde (MW: 168 g mol^{-1}) was assumed to represent the more volatile products, which do not partition to the condensed phase. Because pinonaldehyde resides almost totally in the gas phase, it was not explicitly modelled.

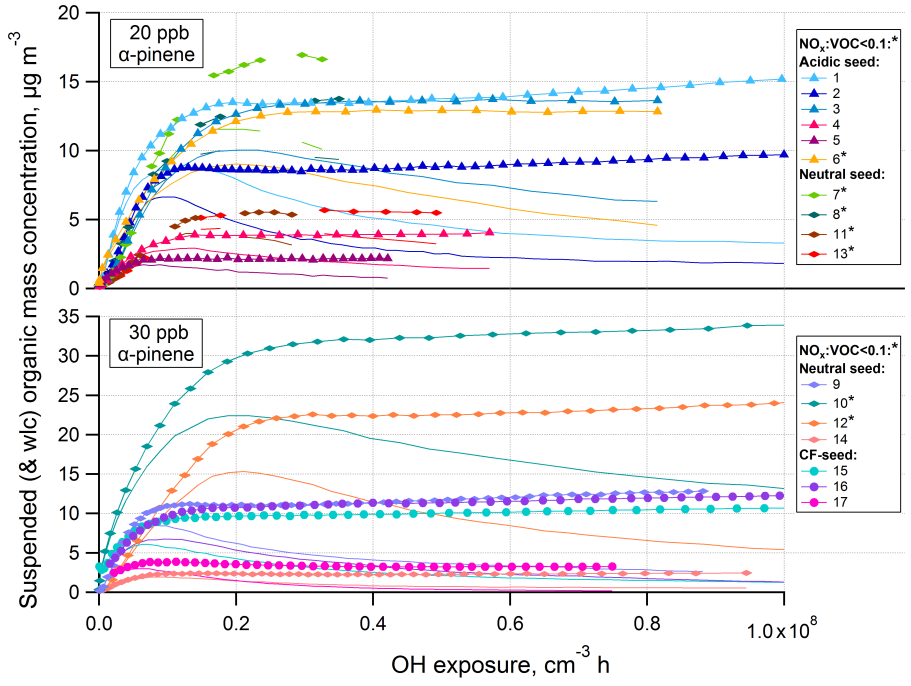

Figure 1. The 20 min averaged wall-loss-corrected (symbols and lines) and suspended (lines) organic mass concentrations as a function of OH exposure. Data are separated according to similar initial α-pinene concentrations (20 ppbv – top panel; 30 ppbv – bottom panel). Experiment numbers are given in the legend and classified by seed composition; asterisks indicate low NO_x experiments.

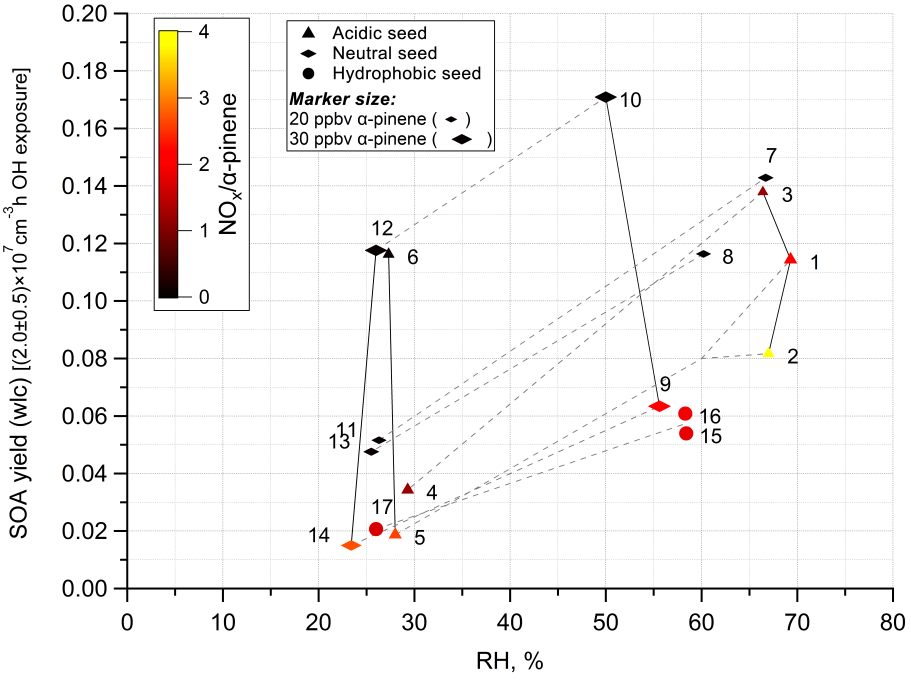

Figure 2. Average wall-loss-corrected yields Y at $(2.0 \pm 0.5) \times 10^7$ cm^{-3} h OH exposure as a function of RH. Symbol sizes represent α-pinene reacted, symbol colours represent NO_x/α-pinene and symbol shapes represent seed composition according to Table 1. Experiments with similar NO_x/α-pinene, seed composition and α-pinene reacted are connected with dashed lines showing the increase in yield for increased RH. Experiment 6 has no counterpart experiment at high RH. Experiments with similar RH, α-pinene reacted and seed composition are connected with solid lines showing the increased yield with a decreasing NO_x/α-pinene ratio.

Model compound C_j^* calculation. Model compounds j were assigned to the volatility bins based on the calculated C_j^* values using Eq. (11) and assuming ideal mixing ($\gamma_j = 1$). Using the actual activity coefficients calculated with AIOMFAC is not possible because they are a result of the phase partitioning calculation. However, because activity coefficients proved to be generally in the range of 0.1 to 10, they did not alter the initial product assignments to the volatility bins, which cover 1 order of magnitude in effective saturation concentration. Therefore, the initial allocation of the compounds to the volatility bins in the VBS remains valid after taking the non-ideality into account. $p^{\circ}_{\mathrm{L},j}$ used in the calculations were vapour pressures of pure compounds in liquid or subcooled liquid state, at 298 K estimated using EVAPORATION (estimation of vapour pressure of organics, accounting for temperature, intramolecular, and non-additivity effects, Compernolle et al., 2011), without using the empirical correction term for functionalized diacids.

Setting model compounds' relative abundances in the model. From the α_i parameters generated through the Monte Carlo simulations in Sect. 2.5, 10 sets per experiment were randomly selected for the phase partitioning calculations (provided that these parameters fall within the 10th and 90th percentiles, to avoid outliers). The 11 chosen experiments exclude experiments 15–17 with hydrophobic seeds, experiment 6 which has no counterpart experiment at high RH, and experiments 5 and 14 where the COA concentration range was very limited to accurately derive α_i parameters (Sect. 2.5). The chosen parameters are listed in Table S5. As several model compounds are assigned to a volatility bin i, the yield of a compound j is expressed as its relative contribution within the volatility bin i, $\chi_{j,i}$, times the relative abundance of the bin α_i. For each experiment and each simulated case the fitted $\chi_{j,i}$ values are listed in Tables S6–S8. For case org the $\chi_{j,i}$ values were optimized to match the experimental organic yields and the measured O : C at the actual RH of the experiment. RH was then changed in the model and the effects of RH on SOA yields and degree of oxygenation were evaluated. For cases id and sd the same $\chi_{j,i}$ were used as for case org. For cases sdfr and orgfr, more fragmented compounds were added and their $\chi_{j,i}$ values were optimized to achieve agreement between measured and modelled organic mass yields and O : C ratios. Likewise, the effects of RH on SOA yields and on O : C ratios were then evaluated by changing the RH in the model.

The following pairs of corresponding experiments were simulated: experiments 3 and 4 (66 % RH, 29 % RH), experiments 7 and 11 (67 % RH, 26 % RH), experiments 8 and 13 (60 % RH, 25 % RH), and experiments 10 and 12 (50 % RH; 26 % RH). Equilibrium calculations were performed starting from both, low and high RH experiments. For experiments 5 and 14 performed at low RH values, the volatility distribution parameters could not be determined for the most volatile bin (α_5). Therefore, equilibrium partitioning calculations were only performed starting from their corresponding experiments, namely experiment 1 (69 % RH), experiment 2 (67 % RH), and experiment 9 (56 % RH).

3 Experimental results

Figure 1 shows the suspended and wall-loss-corrected organic mass concentrations for all experiments listed in Table 1 as a function of OH exposure. SOA mass is rapidly formed and the wall-loss-corrected mass reaches a plateau at an approximate OH exposure of 2×10^7 cm^{-3} h. In the following, comparisons between the different experiments are carried out at an OH exposure of 2×10^7 cm^{-3} h. For illustrative purposes, the wall-loss-corrected aerosol yield is shown in Fig. S8, as a function of α-pinene reacted to demonstrate its variability between different experimental conditions.

3.1 SOA yield dependence on RH, NO_x/α-pinene and aerosol seed composition

In Fig. 2, we examine the relationship between the determined yields and the prevailing experimental conditions: RH, NO_x/α-pinene and seed composition. Lines connect experiments conducted under comparable conditions, but at different RH (dashed lines) and at different NO_x/α-pinene (solid lines). The visible effects of RH and NO_x conditions on the yield in Fig. 2 were statistically examined using a multilinear analysis (Fig. S9 and Table S3). Three yield parameterizations were inter-compared and only the simplest model which represented significantly better the observations was considered for discussion.

The following features can be deduced from the analysis.

1. SOA yields increase with α-pinene concentrations, consistent with the semi-volatile nature of SOA compounds formed. We estimate that yields increase by approximately 2 percentage points when α-pinene concentrations increase from 20 to 30 ppbv.

2. A significant effect of the seed initial concentrations (or surface) on SOA yields was not observed. This may suggest (1) that SOA most likely forms its own phase and does not significantly partition into the seed aerosol (see below) and (2) that SOA condensation is not significantly affected by the vapour losses to the SC walls, which can be diminished by increasing the aerosol surface. This is consistent with recent smog chamber results suggesting that for the α-pinene system SOA formation is dominated by quasi-equilibrium growth and vapour losses to the walls do not depend on the seed concentrations, but rather on SOA (precursor) formation (oxidation) rates (Nah et al., 2016).

3. SOA yields are significantly reduced under high NO_x conditions ($-3.3\,\% \pm 0.6\,\%$, $p < 0.001$), in agreement with literature data (Ng et al., 2007). Such a decrease indicates that SOA compounds formed under low NO_x

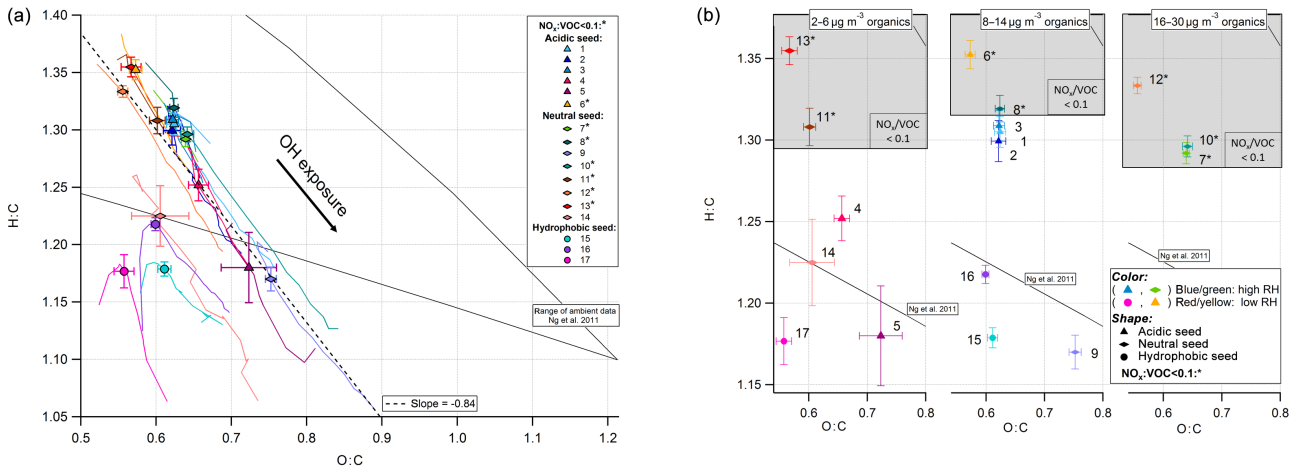

Figure 3. Van Krevelen diagrams: mean (and 1 SD measurement variability) H : C versus O : C at OH exposure $(2.0 \pm 0.5) \times 10^7$ cm^{-3} h (symbols). Symbol colours indicate RH, symbol shapes the seed composition and the asterisk low NO_x experiments. **(a)** The dashed line represents the (least orthogonal distance) fitted slope of experiments (1–14) with inorganic seed: −0.84. The triangular-shaped solid lines represent the range of ambient SOA (Ng et al., 2011a); 1 h averages of H : C versus O : C (for OH exposure $> 2 \times 10^6$ cm^{-3} h) are given by the coloured lines. Experiments 15–17 show the influence of organic seed compounds (data shown from suspended organic mass > 0.3 µg m^{-3}). **(b)** The data were split into three groups according to their wall-loss-corrected organic mass concentrations to exclude concentration effects (left panel: 2–6 µg m^{-3}; middle panel: 8–14 µg m^{-3}; right panel: 16–30 µg m^{-3}). The grey shaded areas include all low NO_x experiments.

conditions are less volatile than those formed under high NO_x conditions.

4. We observed a clear influence of the RH on the yields, which increase on average by 1.5 ± 0.6 % per 10 % RH, for the range explored. This indicates that the particulate water content plays a central role in the partitioning of SOA compounds, either by altering the thermodynamic properties of the bulk phase (e.g. increasing the absorptive mass or decreasing the compound activity coefficients, non-reactive uptake) or by providing a reactive sink for semi-volatile species (e.g. formation of lower volatility compounds/oligomers in the bulk phase, reactive uptake). Additionally, the multilinear analysis suggests that the magnitude of the RH influence on SOA depends on the seed chemical nature (yields correlate with the interaction term between RH and seed composition), with a greater influence for the acidic seed (0.21 ± 0.03 % per 1 % RH, $p < 0.001$), the most hygroscopic aerosol, compared to the non-acidic seed (0.15 ± 0.03% per 1 % RH, $p < 0.001$) and the hydrophobic seed (0.09 ± 0.04 % per 1 % RH, $p = 0.05$).

Overall, these results highlight the sensitivity of SOA yields to the prevailing oxidation conditions and the particle bulk-phase composition and water content and therefore the need to consider such conditions to obtain an accurate prediction of the SOA burden in the atmosphere. Nonetheless, results from this analysis should be regarded with some level of caution, owing to the limited size of the dataset. Despite the methodical assessment of the significance of the multilinear analysis results, we cannot unambiguously propose a mechanism by which water and seed hygroscopicity/acidity enhance SOA yields or determine whether there is interplay between these two parameters. Nevertheless, we provide evidence that both of these parameters play a significant role in the formation or condensation of SOA species. In Sect. 4, using phase partitioning computation and AIOMFAC, we shall assess to what extent and under which conditions particulate water may alter the organic species' activity coefficients and as a consequence their absorptive partitioning.

3.2 SOA elemental composition

The effect of the experimental conditions on SOA chemical composition was investigated using the Van Krevelen space (Fig. 3a). The overall region of the experimental data is very comparable for all experimental conditions and comparable to ambient data (Ng et al., 2011a). Data for experiments 1–14, with inorganic seeds, follow a similar slope with aging (−0.84): an increase in O : C during aerosol aging takes place under all conditions. The O : C and H : C ratios of SOA produced with hydrophobic seed aerosol (experiments 15–17) show lower values than with inorganic seeds.

In Fig. 3b, data are separated according to the wall-loss-corrected organic mass concentrations C_{OA} (left panel: 2–6 µg m^{-3}; middle panel: 8–14 µg m^{-3}; right panel: 16–30 µg m^{-3}), to isolate the NO_x and RH effects on the chemical composition from the possible influence of enhanced partitioning of semi-volatile organic species to the aerosol phase due to a higher SOA loading (Pfaffenberger et al., 2013). We observe that NO_x levels have the highest influence on SOA elemental composition; namely, SOA formed at low

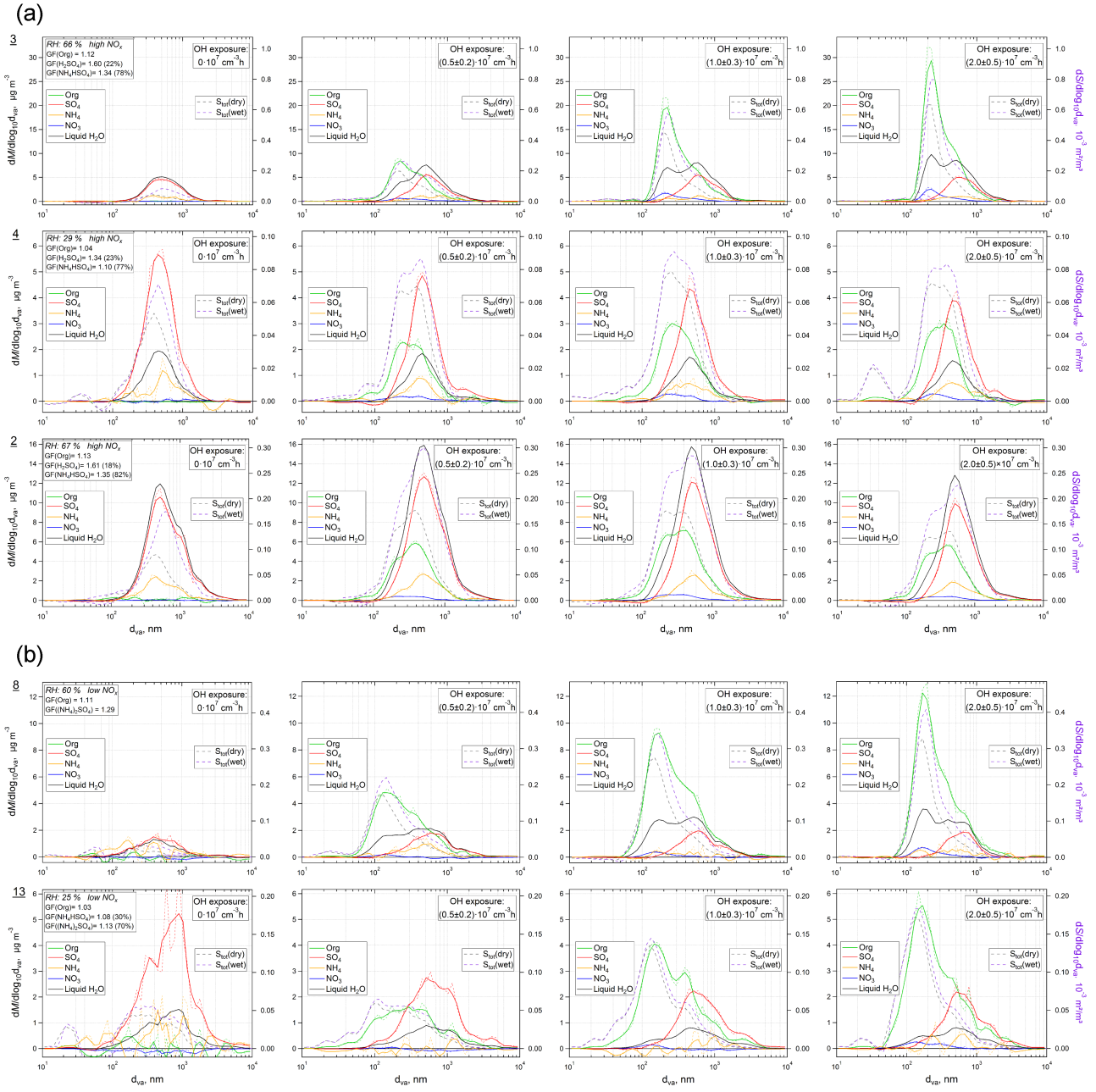

Figure 4. Evolution of size distributions from the HR-ToF-AMS. Measured organic, SO_4, NH_4, and NO_3 mass distributions for OH exposures of $0\times$, $(0.5\pm0.2)\times$, $(1.0\pm0.3)\times$ and $(2.0\pm0.5)\times10^7$ cm^{-3} h. Black lines represent estimated liquid water content (method: Sect. 2.3; RH and individual GFs given in the legend, percentage in brackets: fractions of SO_4). The calculated dry and wet surface distributions are shown as dashed lines on the right axes. **(a)** High NO_x with more acidic seed [H_2SO_4 and NH_4HSO_4]: experiments 3 and 4 with NO_x/α-pinene = 1.2 and experiment 2 with NO_x/α-pinene = 3.8. **(b)** Low NO_x with less acidic seed [$(NH_4)_2SO_4$ and NH_4HSO_4]: experiments 8 and 13 with NO_x/α-pinene $\approx$ 0.05. Additional figures in the Supplement (Fig. S12).

NO_x (marked with asterisks) is characterized by higher H : C than that formed at high NO_x. This is even more pronounced at an early reaction stage (OH exposure $<2\times10^6$ cm^{-3} h, not shown in Fig. 3), where fresh SOA products formed during all low NO_x experiments have higher H : C and lower O : C. Such an influence of NO_x levels on SOA elemental composition is consistent with our general understanding of gas-phase chemistry: under low NO_x, substantial amounts of hydroperoxides and alcohols would result in a higher H : C ratio than e.g. carbonyls formed under high NO_x conditions (Atkinson, 2000). Also, as hydroperoxides and alcohols are substantially less volatile than carbonyls and less fragmen-

tation is expected at lower NO_x conditions, less oxygenated species with higher carbon numbers may partition to the particle phase at low NO_x, which would lead to lower O : C ratios.

NO_x levels also affect the amount of organonitrate formed. Assuming that the entire nitrate signal arises from organonitrates (i.e. a maximum organonitrate contribution), we estimate molar ratios (Fig. S10) of NO_3 to carbon of $\sim 1:30$ for high NO_x and $\sim 1:100$ for low NO_x. Assuming oxidation product molecules with 10 carbon atoms, these ratios imply that every 3rd and 10th molecule contains one NO_3 functional group, for high and low NO_x conditions, respectively.

Conversely, we could not observe a significant effect of RH and seed composition on SOA elemental composition and degree of oxygenation, despite their significant influence on SOA yields. This may be due to the limited range of the O : C ratio spanned by the different experiments in our case (on average $O:C \in [0.56-0.75]$ at an OH exposure of 2×10^7 cm^{-3} h). Furthermore, we did not observe any significant dependence between these parameters and the ratio of organic fragments larger than m/z 150 to the total organic mass, a proxy for oligomers measured with the HR-ToF-AMS, which would explain the observed increase in yields with the aerosol liquid water content (Fig. S11).

3.3 Analysis of aerosol size-resolved chemical composition

As the seed composition and particulate water content appear to greatly influence SOA yields, we examine in this section the interaction between these parameters and SOA, through the investigation of the aerosol size-resolved chemical composition. This information is used later to infer the behaviour of the absorptive organic phase and its mixing with the inorganic seed, while modelling the aerosol dynamics in the SC is beyond the scope of this study. Figure 4 shows the aerosol size-resolved chemical composition at 0×10^7, $(0.5\pm0.2)\times10^7$, $(1.0\pm0.3)\times10^7$ and $(2.0\pm0.5)\times10^7$ cm^{-3} h OH exposure for five experimental conditions (data for additional experiments are available in Fig. S12). Figure S13 shows a 3-D representation of the time-dependent number and volume size distributions, measured by the SMPS.

For all experiments, the aerosol size distributions show two externally mixed aerosol populations, with a mode at lower diameters ($\sim$ 200 nm, mode 1) mostly containing SOA and another mode at higher diameters ($\sim$ 400 nm, mode 2) mostly consisting of the seed. We note that the particle size distribution evolved consistently under different conditions, with the smallest seed particles growing with SOA condensation or coagulation (Figs. S12 and S13). While we have detected an increase in particle number (Fig. S14), we note that intense nucleation events did not occur. For higher yields, the main SOA mass occurs in mode 1 and despite the sizeable increase in the yield with particulate water content (e.g. under acidic conditions and high RH), we did not observe a significant enhancement of SOA in mode 2. In addition, we did not note any statistically significant correlation between the initial seed volume and SOA yields; instead SOA growth seems to be driven by the favourable partitioning of semivolatile species to smaller particles at an early stage of the experiment (Fig. 4). Such behaviour would imply that semivolatile compounds do not additionally partition or react in the electrolyte-rich phase on the timescale of this experiment, but rather the reactive or non-reactive uptake of these products onto the particles is enhanced with the increase in the initial particulate water content.

3.4 Prevalent oxidation reagent and its influence on SOA yields and chemical composition

Based on the mixing ratios of OH and ozone, we estimate that a greater part of α-pinene has reacted with OH (on average 0.78 ± 0.07). Moreover, it is worthwhile mentioning that the further processing of the first-generation products – which do not contain $C=C$ bonds – would almost exclusively proceed through OH oxidation. Accordingly, we conclude that SOA compounds detected are mainly from OH chemistry, independent of the NO_x level and relative humidity.

We note that the fractions of α-pinene that reacted with OH under low RH (0.79 ± 0.07) and high RH (0.77 ± 0.07) are not statistically different (t test, $p=0.71$), within our experimental variability. Therefore, we do not expect that differences in SOA yields observed between experiments at low and high RH will be due to a change in the prevalent oxidant. We recognize that water vapour may change the oxidation product distributions, via its reaction with the stabilized Criegee intermediates, produced upon the ozonolysis of α-pinene. However, we note that not only the fraction of α-pinene that reacts with O_3 is not substantial (in comparison with that reacted with OH), but a major fraction of α-pinene Criegee intermediates also undergoes unimolecular decomposition to form OH and does not react with water (Atkinson and Arey, 2003). Therefore, it is unlikely that a change in RH would sizably modify the distribution of the products formed via gas-phase chemistry.

By contrast, the fraction of α-pinene that reacted with OH is found to be sensitive to the NO_x concentration. The production of O_3 was faster under high NO_x (average $[O_3]=35$ ppbv) compared to low NO_x (average $[O_3]=22$ ppbv), due to an efficient VOC–NO_x catalytic cycle. Consequently, the fraction of α-pinene that reacted with OH under high NO_x (0.75 ± 0.06) is lower than that under low NO_x (0.83 ± 0.04). These small but statistically significant differences (8 percentage points; t test, $p=0.004$) in the contribution of ozone/OH to α-pinene oxidation are expected to explain a small part of the differences in SOA yields and chemical composition observed at low and high NO_x, with a higher fraction of ozonolysis products under high NO_x conditions. Despite this, we expect the influence of NO_x on the

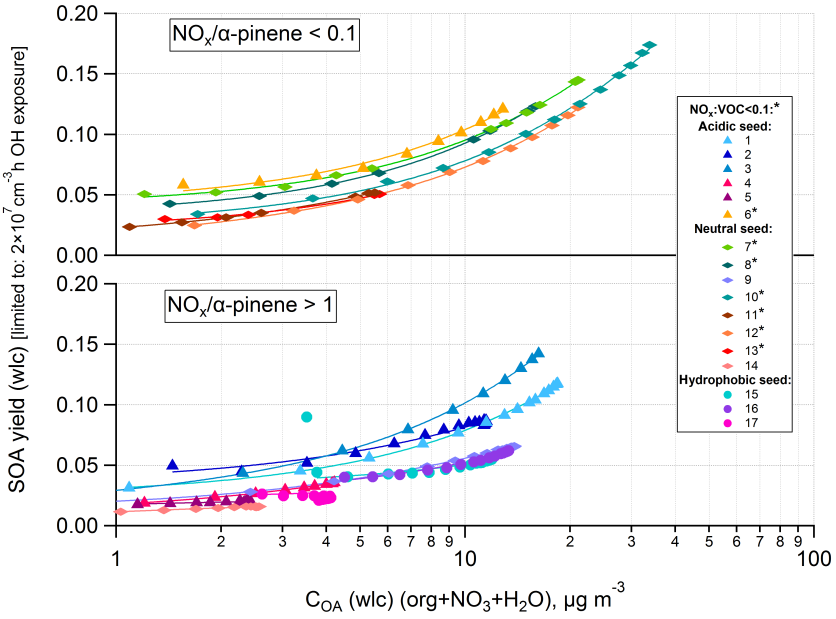

Figure 5. Measured (symbols) and parameterized (lines) wall-loss-corrected SOA yield, Y, as a function of wall-loss-corrected absorptive mass concentration (C_{OA}: organics + NO_3 + H_2O) for low NO_x experiments (upper panel) and high NO_x experiments (lower panel). Data were limited to an OH exposure of 2×10^7 cm^{-3} h and averaged over 20 min. Symbol colours indicate the RH, symbol shapes the seed composition and the asterisks the NO_x / VOC ratio.

fate of RO_2 to be the main driver of the observed differences in SOA yields and chemical composition between low and high NO_x conditions (because ozonolysis products are only a minor fraction and differences between the two conditions are rather small).

4 Phase partitioning calculation results

The organic yields and O : C ratios of the phase partitioning calculations are presented in Figs. 7 and 8, respectively, and listed in Table S9. Each panel in Fig. 7 compares organic yields for the cases org, id, sd, sdfr, and orgfr at the actual RH of the experiment (full colour) and at the lower/higher RH of the corresponding experiment (light colour). Table 2 gives the increase in organic yields from low to high RH of the corresponding experiments as ratios (org yield (high RH)/org yield (low RH)).

The main objectives of the phase partitioning calculations are (1) estimating the impact of liquid water on SOA mixing properties (activity coefficients and liquid–liquid phase separation (LLPS)) and (2) determining the conditions or the potential model mixtures that can explain the observed yields and O : C ratios and their variation with RH. We note that model results are highly sensitive to the surrogates assumed, and the determination of SOA composition on a molecular level would considerably help in confirming our results. Nevertheless, fitting both organic yields and O : C ratios significantly aids in constraining the type of compounds that participate in partitioning (i.e. from a compound O : C ratio and vapour pressure, its carbon number can be inferred). For example, highly oxygenated compounds cannot be very volatile without significant fragmentation, whereas oligomerization leads to a significant decrease in the compounds' vapour pressure without necessarily increasing their O : C ratios.

4.1 Simulations with reported α-pinene photo-oxidation products (cases org, id, sd)

For case org, the contribution of model compounds ($\chi_{j,i}$) to the volatility bins at the actual RH could be optimized such that agreement was achieved between measured and calculated yields with deviations of less than 10 %, constituting a proof of concept of the applied approach. For most simulations, the $\chi_{j,i}$ values optimized for case org were also valid for cases id and sd.

In general, simulations assuming cases org, id and sd failed in predicting the change in SOA yields with RH (Fig. 7) and led to a significant underestimation of the SOA O : C ratios (Fig. 8). The only exception is the pair of experiments 10 and 12 performed at low NO_x (1.9 ppbv) and high α-pinene levels (30.4 ppbv) for which the model could account for 87–99 % of the increase in SOA yield from low to high RH. This agreement was achieved although the model underestimated the O : C ratios by 24 % and predicted a smaller increase in the O : C values with RH than observed. The modelled O : C remained almost constant at 0.45–0.48 at low and high RH (difference of 6 %), while the measured O : C increased from

Table 2. Increase in organic yield from low to high RH for the different experiments as org yield (high RH)/org yield (low RH). The second column lists the ratio of measured organic yield enhancements with RH. In the five last columns the ratios of organic yields calculated at high and low RH for the different experiments are given (average value of the 10 volatility distributions with lowest and highest values in brackets in the second row).

Experiments		Calculations					
Exp. no.	Yield ratio	Exp.	Case org	Case id	Case sd	Case sdfr	Case orgfr
1/5	6.38	1	1.62	2.02	1.54	4.23	4.34
			(1.48–1.86)	(1.67–2.57)	(1.37–1.77)	(2.50–6.70)	(2.89–6.62)
2/5	4.10	2	1.42	1.61	1.31	2.74	2.24
			(1.23–1.47)	(1.31–1.73)	(1.18–1.35)	(1.33–6.24)	(1.35–2.92)
3/4	3.23	3	1.64	2.07	1.57	3.67	3.13
			(1.44–1.86)	(1.88–2.38)	(1.48–1.73)	(2.74–5.29)	(2.53–4.14)
3/4	3.23	4	1.76	2.09	1.58	2.93	3.12
			(1.58–1.90)	(1.78–2.41)	(1.44–1.71)	(1.91–4.88)	(2.13–4.09)
7/11	2.95	7	1.35	1.52	1.28	2.16	2.38
			(1.25–1.47)	(1.35–1.80)	(1.20–1.39)	(1.48–3.98)	(1.64–3.69)
8/13	2.32	8	1.43	1.61	1.36	2.66	2.44
			(1.30-1.58)	(1.43-1.87)	(1.27-1.50)	(1.60-4.79)	(1.73-3.57)
9/14	4.63	9	1.43	1.56	1.33	2.45	2.69
			(1.32–1.59)	(1.38–1.82)	(1.23–1.48)	(1.61–4.70)	(1.75–4.24)
10/12	1.46	10	1.29	1.38	1.28	1.44	1.55
			(1.13–1.52)	(1.22–1.67)	(1.17–1.49)	(1.18–1.66)	(1.26–2.17)
7/11	2.95	11	1.80	2.22	1.67	2.74	3.38
			(1.52–2.21)	(1.69–3.09)	(1.40–2.05)	(1.75–4.03)	(1.87–5.61)
10/12	1.46	12	1.34	1.48	1.33	1.34	1.70
			(1.21–1.48)	(1.27–1.71)	(1.19–1.49)	(1.19–1.65)	(1.33–2.06)
8/13	2.32	13	1.54	1.74	1.41	2.73	2.54
			(1.39–1.68)	(1.52–1.91)	(1.30–1.50)	(1.29–6.06)	(1.39–4.90)

0.56 at low RH to 0.64 at high RH (change of 14 %). We also note that the use of the more recent parameterization by Canagaratna et al. (2015) would yield even higher O : C values, widening the gap between measured and modelled O : C ratios.

For the other experiments performed under low NO_x conditions, model simulations accounted for only 43–75 % of the observed yield increase with RH. Simulated O : C values ranged from 0.48 to 0.55 and failed to reproduce the observed increase from 0.57 to 0.62 for experiments 8 and 13 and from 0.6 to 0.64 for experiments 7 and 11. Likewise, for high NO_x conditions, model simulations for experiments 1 and 5, 2 and 5 and 9 and 14 could only account for 24–39 % of the observed yield increase from low to high RH and for 49–65 % for experiments 3 and 4. Simulated O : C values remained almost constant at 0.49–0.54 for all high NO_x experiments and were considerably lower than the observed O : C ratios.

For case id the increased SOA yield at high RH, attributed to the additional partitioning of semi-volatile compounds (norpinic acid, 2-hydroxyterpenylic acid, 10-oxopinonic acid and 4-oxopinonic acid), is a direct consequence of the increased absorptive mass due to the higher water content. For cases org and sd, partitioning to the condensed phase is reduced compared to case id as AIOMFAC predicts activity coefficients greater than 1 for higher-volatility compounds, e.g. 10-oxopinonic acid and 4-oxopinonic acid. This effect is even enhanced for case sd, when partitioning to the total condensed phase including the seed aerosol is simulated. Although LLPS is predicted for all simulations, the salting-out effect of AS which also partitions to some degree to the organic phase leads to a further decrease in the organic yield at high RH compared to case id.

In summary our results suggest that with the reported model compounds for α-pinene photo-oxidation, the measured O : C and the increase in organic yields with RH cannot be simulated. Therefore, we explored whether the formation of fragmented and more oxidized products may explain the high O : C ratio observed and the high sensitivity of the yields to RH.

4.2 Simulations including fragmented products (cases sdfr and orgfr)

Non-fragmented products (e.g. highly oxygenated C10 or dimers) would be low-volatility (LVOC) or extremely low-volatility organic compounds (ELVOC) (Zuend and Seinfeld, 2012; Donahue et al., 2006, 2012b; Tröstl et al., 2016) with effective saturation concentrations $C^* \leq 0.1\,\mu g\,m^{-3}$, when

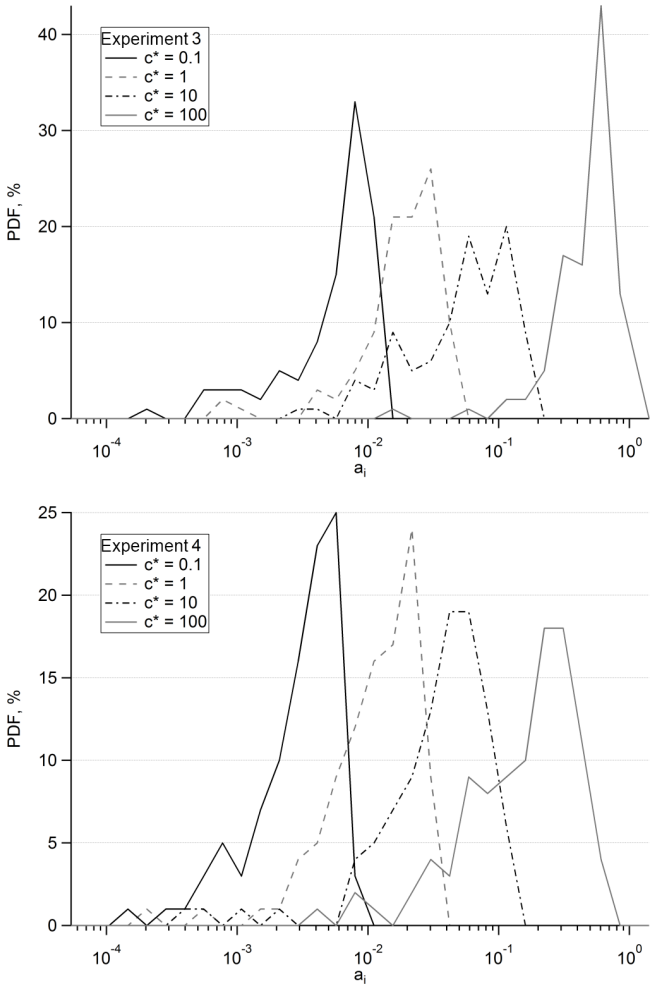

Figure 6. Probability density functions (PDFs) of α_is for volatility bins ($C_i^* = 0.01$, 0.1, 1, 10 and 100 µg m^{-3}) for one high RH (exp. 3, upper panel) experiment and one low RH (exp. 4, lower panel).

their O : C ratio is as high as the observed O : C ratio. Therefore, they are expected to be in the particle phase independent of the prevalent RH and the inclusion in the model of additional amounts of these products would not help explain the observed difference in the yields at different RHs, leading to an overestimation of OA mass at low RH. This implies that to better capture the measured O : C range without overestimating SOA yields, fragmented products with shorter backbones need to be introduced.

Low molecular weight compounds resulting from fragmentation were therefore added to the volatility bins with $C^* = 1$–100 µg m^{-3}, namely, 3-oxoadipic acid to the volatility bin with $C^* = 1$ µg m^{-3}, glutaric acid to the volatility bin with $C^* = 10$ µg m^{-3} and 5-COOH-3-OH-pentanal and succinic acid to $C^* = 100$ µg m^{-3}. For case sdfr, α_i parameters were optimized assuming equilibrium partitioning of SOA to the whole condensed phase, including the seed aerosol. For case orgfr absorption to the organic phase only was assumed. While the organic and inorganic phases seem to form externally mixed particles based on the chemically resolved size distribution, examining both cases provides valuable insights into the impact of the presence of an inorganic aerosol seed in the system. Tables S7 and S8 of the Supplement provide the contribution of model compounds ($\chi_{j,i}$ values) to volatility bins C_i^* for these cases. The organic yields and O : C ratios for cases sdfr and orgfr are shown in Figs. 7 and 8, respectively. In Table 2 the relative increase in SOA yields from low to high RH is given. Cases sdfr and orgfr are similarly successful in reproducing SOA yields and O : C ratios. However, the variability in the modelled yields when using different volatility distributions for cases sdfr and orgfr is larger than for cases org, id, and sd (Fig. 7).

For experiments carried out at low NO_x conditions (experiments 7 and 11, 8 and 13 with $NO_x < 2$ ppbv), both cases explained the observed increase in the organic yields with RH and improved the agreement between modelled and observed O : C ratios. For experiments 8 and 13, both cases accurately captured the increase in SOA yields from low to high RH with deviations < 2 %. Modelled O : C agreed very well with measurements for case sdfr with deviations ≤ 1 % and slightly worse for case orgfr with deviations of ≤ 5 %. For experiments 7 and 11, cases sdfr and orgfr reproduced satisfactorily (deviations ≤ 11 %) the measured yields for calculations with the volatility distributions determined for experiment 11, but overestimated the observed increase in O : C from low (O : C = 0.60) to high RH (O : C = 0.64). Using the volatility distributions determined for experiment 7, the low yields at low RH could not be achieved. For experiments 10 and 12, cases org, id, and sd were able to simulate the increase in organic yield with the oxidation products reported in the literature, but failed to reproduce the observed O : C ratios. Cases sdfr and orgfr with additional oxidized and fragmented products showed improved agreement of observed yields and reproduced successfully the observed O : C ratios.

Under high NO_x conditions, cases sdfr and orgfr could only simulate satisfactorily SOA yields and O : C ratios observed during experiments 3 and 4. For experiments 1–2 and 5, and 9 and 14, model and measurement agreement was less satisfactory. The model could not reproduce the low yields at low RH observed during experiments 5 and 14, and hence the strong reduction of the yields observed with the decrease in RH is underestimated (the simulations predict only 52–66 % of the observed change). Additionally, for these experiments the model underestimates the O : C ratios (average measured O : C = 0.66 and 0.68, at low and high RH, respectively). In the following, we examine and discuss the potential reasons that might explain model–measurement disagreements.

4.3 Simulations including organonitrates

We examined whether the discrepancy between modelled and measured yields may be ascribable to the selection of

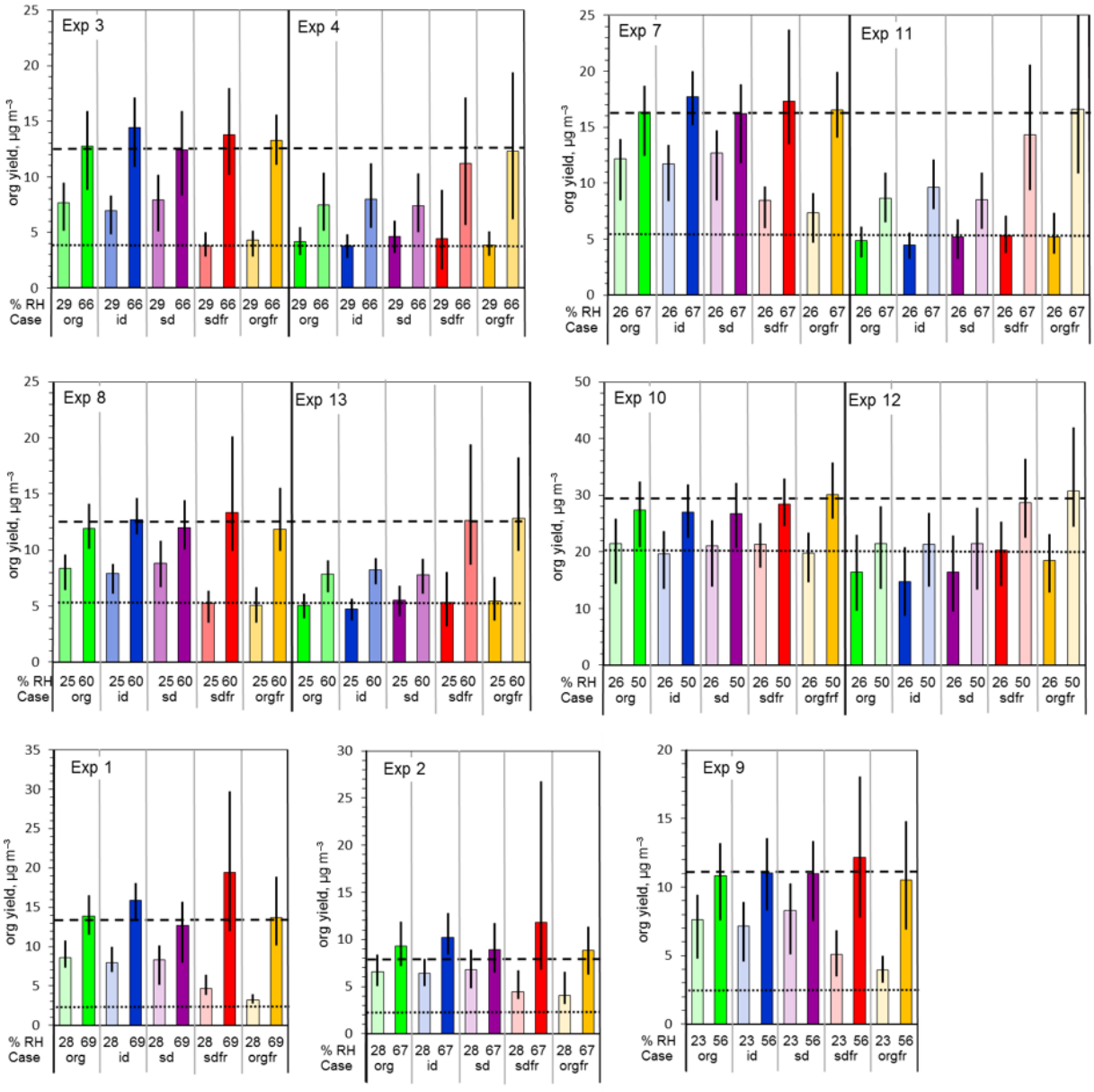

Figure 7. Calculated average organic yields for experiments at the measured RH (columns in full colours) and at the RH of the corresponding experiments (light colours; see Table 2 for reference) based on 10 randomly chosen volatility distributions for the cases org, id, sd, sdfr, and orgfr (identified by different colours). The vertical black lines in the columns indicate the range of values obtained for the calculations with the individual volatility distributions. The horizontal dotted line marks the measured value for the experiment performed at low RH, the dashed line the value for the experiment performed at high RH.

the model compounds at high NO_x, by introducing additional surrogates – specifically organonitrates – expected to be representative of the compounds formed under these conditions. Assuming that the NO_3 signal in the HR-ToF-AMS originates from organonitrates, every third molecule should contain one ONO_2 functional group at high NO_x conditions. We tested whether adding organonitrates described by Valorso et al. (2011) would improve the agreement between measurements and observations for the high NO_x experiments. However, this was not the case (not shown). Such sensitivity tests could not be performed for cases including partitioning to the seed aerosol because interaction parameters between organonitrates and sulfate are not available in AIOMFAC.

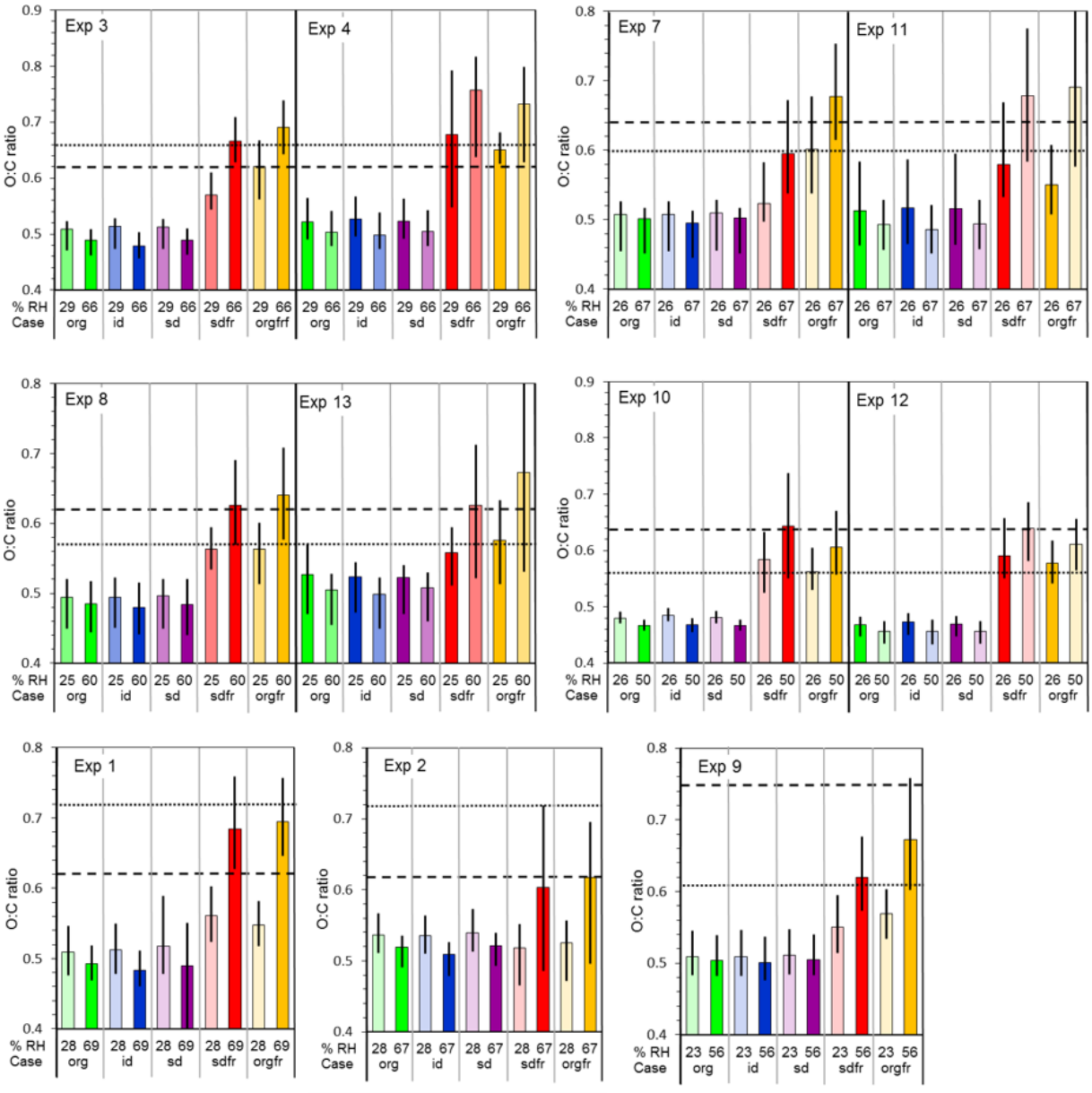

Figure 8. Calculated average O : C ratios for experiments at the measured RH (columns in full colours) and at the RH of the corresponding experiments (light colours; see Table 2 for reference) based on 10 randomly chosen volatility distributions for the cases org, id, sd, sdfr, and orgfr (identified by different colours). The vertical black lines in the columns indicate the range of values obtained for the calculations with the individual volatility distributions. The horizontal dotted line marks the measured value for the experiment performed at low RH, the dashed line the value for the experiment performed at high RH.

4.4 Simulations including higher volatility oxidation products

The Monte Carlo simulations enabled the determination of α_i parameters for volatility bins $C^* = 0.1$–$100\,\mu g\,m^{-3}$. α_i parameters in the volatility bin with $C^* = 1000\,\mu g\,m^{-3}$ could not be reliably extracted. Nevertheless, SOA products belonging to this bin are present in the chamber and could partition to some extent to the condensed phase. We investigated whether the presence of substances with an effective saturation concentration of $1000\,\mu g\,m^{-3}$ could reproduce the low SOA yields at low RH and its strong increase at high RH observed for the high NO_x experiments 1 and 5, 2 and 5, and 9 and 14. This was achieved by replacing a part of the substances in the volatility bin $C^* = 100\,\mu g\,m^{-3}$ with pinalic acid, terpenylic acid and 3-2-oxopropanylolxypropanoic acid (Table S4). While the addition of these compounds in the model could reproduce the low yields at low RH, the yields at

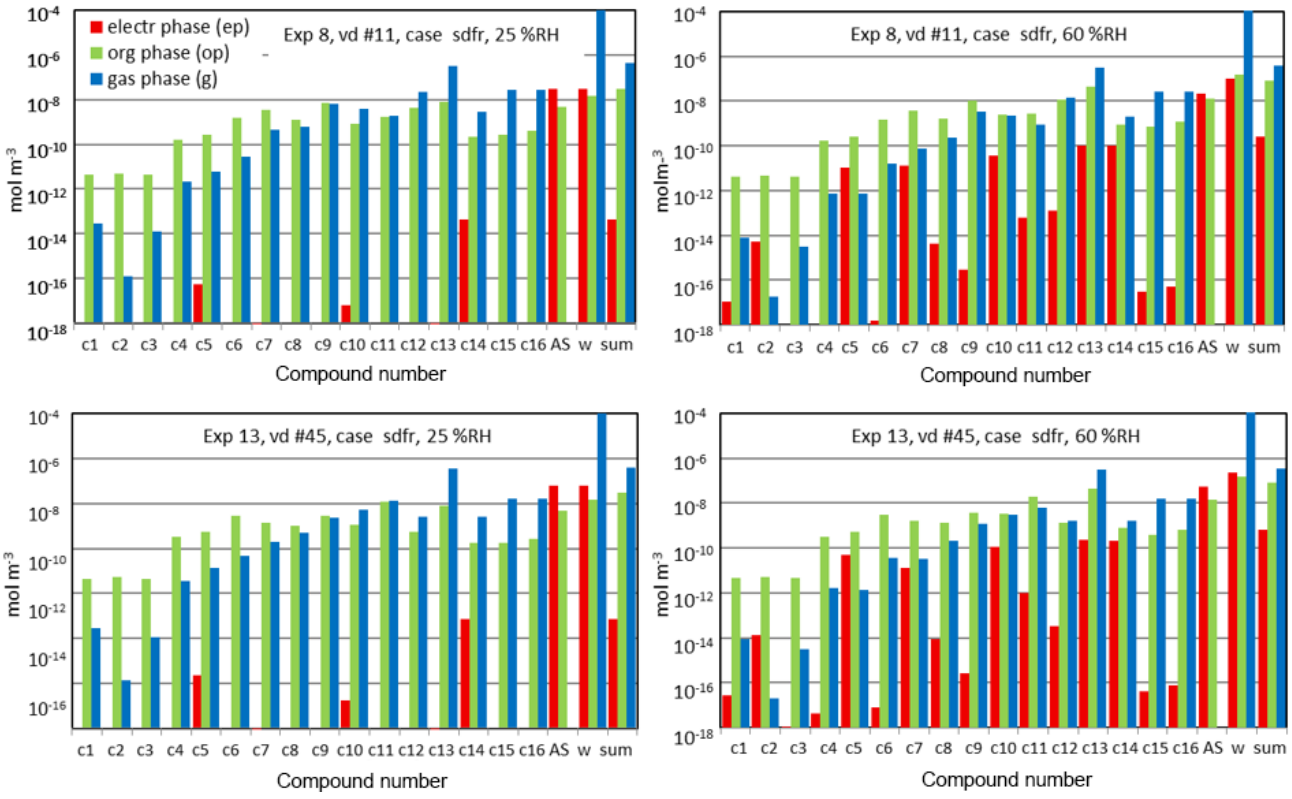

Figure 9. Equilibrium phase partitioning (mol m^{-3}) for case sdfr between gas phase, electrolyte phase, and organic phase at low RH (25 %) and at high RH (60 %) for experiment 8, volatility distribution 11 (upper panels) and experiment 13, volatility distribution 45 (lower panels). Compound numbers are c1: diaterpenylic acid acetate, c2: 3-MBTCA, c3: ValT4N9, c4: ValT4N10, c5: 3-hydroxyglutaric acid, c6: ValT4N3, c7: 3-oxoadipic acid, c8: pinic acid, c9: hopinonic acid, c10: glutaric acid, c11: norpinic acid, c12: 2-hydroxyterpenylic acid, c13: 5-COOH-3-OH-pentanal, c14: succinic acid, c15: 10-oxopinonic acid, c16: 4-oxopinonic acid, ammonium sulfate (AS), water (w), and the sum of the compounds c1–c16.

high RH were strongly underestimated (not shown). Accordingly, the introduction of organonitrates or higher-volatility compounds in the model did not improve the agreement between modelled and observed yields and O : C ratios (not shown here), suggesting that equilibrium partitioning alone cannot explain the strong SOA yield increase under high NO_x conditions.

4.5 Partitioning of individual components into the gas and condensed phases

The phase partitioning calculations do not only allow the simulation of the total organic yield and average O : C ratio of the condensed products, but also provide insights into the partitioning of individual compounds to the gas and condensed phases. Phase partitioning of individual model compounds into the gas and condensed phases for case sdfr is examined in Fig. 9 for experiments 8 and 13 and in Fig. 10 for experiments 3 and 4. Detailed results of the phase partitioning calculations are listed in Tables S10 and S11. For experiments 8 and 13, the model predicts an LLPS into an organic-rich phase (op) and a predominantly electrolyte-like phase (ep). Overall, organic compounds are predominantly in the organic phase at both RH, with ep/op $< 1 \times 10^{-5}$ at 25 % RH, and ep/op ≈ 0.003–0.008 at 60 % RH. Compounds in volatility bins $C^* = 0.01$ and $0.1\,\mu g\,m^{-3}$ are mainly present in the condensed phases, while compounds in volatility bin $C^* = 100\,\mu g\,m^{-3}$ show preferred partitioning to the gas phase. The strongest increase in the condensed phase when RH is increased from 25 to 60 % is observed for the model compounds assigned to $C^* = 100\,\mu g\,m^{-3}$. Moderately oxygenated species (4-oxopinonic acid and 10-oxopinonic acid) in this bin show a moderate increase (about a factor of 2) driven by the increase in the absorptive mass. This increased partitioning is limited by an increase in the activity coefficients of these compounds (for experiment 8 from 1.69 and 1.63 at low RH to 2.70 and 2.93 at high RH and for experiment 13 from 1.49 and 1.54 at low RH to 2.88 and 3.24 at high RH). Conversely, the 5-fold enhanced partitioning of the fragmented and more functionalized compounds (5-COOH-3-OH-pentanal and succinic acid) into the condensed phase at high RH is driven by the increase in the absorptive mass and the slight decrease in the compounds' activity coeffi-

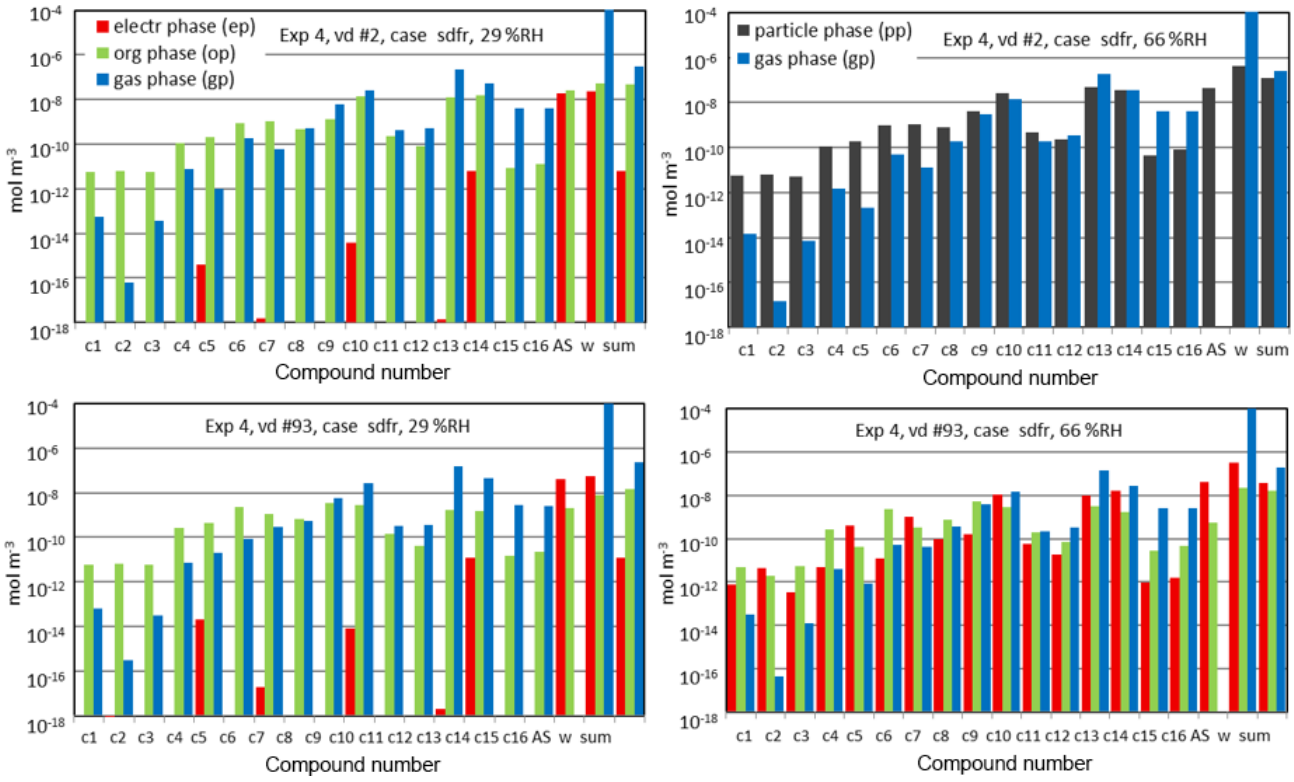

Figure 10. Equilibrium phase partitioning (mol m^{-3}) for case sdfr between gas phase, particle phase, electrolyte phase, and organic-rich phase at low (29 %) and high (66 %) RH for experiment 4, volatility distribution 2 (upper panels), and volatility distribution 93 (lower panels). Compound numbers are c1: diaterpenylic acid acetate, c2: 3-MBTCA, c3: ValT4N9, c4: ValT4N10, c5: 3-hydroxyglutaric acid, c6: ValT4N3, c7: 3-oxoadipic acid, c8: pinic acid, c9: hopinonic acid, c10: glutaric acid, c11: norpinic acid, c12: 2-hydroxyterpenylic acid, c13: 5-COOH-3-OH-pentanal, c14: succinic acid, c15: 10-oxopinonic acid, c16: 4-oxopinonic acid, ammonium sulfate (AS), water (w), and the sum of the compounds c1–c16.

cients (for experiment 8 from 0.84 and 0.51 at low RH to 0.68 and 0.43 at high RH and for experiment 13 from 0.90 and 0.56 at low RH to 0.69 and 0.44 at high RH).

For experiments 3 and 4, model results obtained from the parameterization of the yields in experiment 4 are highly sensitive to the assumed volatility distribution. As shown in Fig. 10, when introducing volatility distributions characterized by high contributions of semi-volatile oxygenated compounds pertaining to the volatility bin $C^* = 100\,\mu g\,m^{-3}$, the model predicts a liquid-phase mixing. Note that when mixing is predicted, the model tends to overestimate the O : C ratio (O : C = 0.81 at high RH for volatility distribution 2 shown in the upper panels of Fig. 10) and the yields at both high and low RH. Conversely, when volatility distributions with less volatile and less oxygenated compounds are used (e.g. volatility distribution 93), lower yields and lower O : C ratios (0.69 for volatility distribution 93 shown in the lower panels of Fig. 10) are obtained and LLPS is predicted. For such O : C ratios LLPS has also been observed for experiments performed with model mixtures (e.g. Song et al., 2012). For experiment 4, the volume of the electrolyte phase is larger than that of the organic-rich phase and there is considerable partitioning of organic compounds to the electrolyte phase (ep/op = 2.26). These observations illustrate that for compounds with high O : C ratios, small differences in the volatility distribution parameters can lead to totally different phase partitioning. Irrespective of these differences, none of the volatility distributions used could reproduce the measured yields at both high and low RH, likely due to the deficient representation in the model of the interactions between the acidic aerosol and the organic compounds – and of the chemical processes occurring under acidic/high NO_x conditions.

4.6 Modelling considerations and limitations

Model simulations were carried out by considering two α-pinene C8–C10 photo-oxidation products per volatility bin for cases org, id and sd. This number was sufficient to represent the species within one volatility bin, because the hydrophilicity of these compounds with a consistently high carbon number correlates with their volatility. Therefore the sensitivity of model predictions to the contribution of these compounds to the volatility bins (described by $\chi_{j,i}$ values) is relatively low. This model setting, corresponding to a pseudo-

one-dimensional VBS where the compounds' vapour pressure and degree of oxidation correlate, was proven to be insufficient for an accurate description of both SOA mass and degree of oxygenation. By contrast, for cases sdfr and orgfr, which include more oxidized short chain products, hydrophilicity and volatility may be varied more independently, which introduces an additional degree of freedom and would correspond to a pseudo-two-dimensional VBS (2D-VBS), as described by Donahue et al. (2011). While we show that model predictions based on this setting are highly dependent on the volatility distribution parameters and model compounds assumed, in general the introduction of fragmented more oxidized compounds reproduced well the high observed O : C ratios and the increase in O : C and SOA yields with RH, specifically at low NO_x. The estimated volatility distributions and average carbon (C$\sim$ 6) and oxygen (O$\sim$ 4) numbers when considering fragmented products are in agreement with chemical speciation analysis previously reported for the same system (Chhabra et al., 2015). The analysis shows that for such semi-volatile products with O : C ratios of the order of $\sim$ 0.6, an increase in RH from 23–29 to 60–69 % induces a mass increase by up to a factor of 3, driven by the higher particle water content and the lower activity coefficients of the more fragmented products at high RH.

The measured O : C ratio is a key parameter for constraining the model. Here, we have used the high-resolution parameterization proposed by Aiken et al. (2007), while the use of the more recent parameterization by Canagaratna et al. (2015) would result in even higher O : C ratios (by 18 %). Higher O : C ratios would require increasing even further the contribution or the degree of oxidation of the fragmented compounds and would imply that the model predicts an even higher sensitivity of the yields to RH. Therefore, the O : C values used here yield more conservative estimates of the contributions (or the degree of oxidation) of fragmented products in the model and of the sensitivity of the yields and O : C ratios to the RH.

Under high NO_x (and low pH), the model could not reproduce the factor of 6 increase in yields at high RH, using a variety of chemically dissimilar surrogate compounds. This indicates that the increased absorptive uptake of these compounds due to the increase in SOA mass and the decrease in the compounds' activity coefficients cannot explain the observed enhancements alone. Under these conditions, additional processes may likely play a role in the enhancement of OA with RH. NO_x concentrations have a dramatic influence on SOA chemical composition and volatility. Therefore, the discrepancy between model and measured yields at high NO_x conditions may be explained by either an inadequate representation of SOA surrogates in the model and their interaction parameters with the seed or by an enhanced reactive uptake of SOA species formed under high NO_x conditions, such as carbonyls that are reported to instigate the formation of lower-volatility compounds in the particle phase (Shiraiwa et al., 2013, and references therein). Given the dearth of additional chemically resolved measurements of the particle-phase species formed under different conditions, the mechanism by which RH enhances the uptake of SOA species under high NO_x (low pH) remains currently undetermined.

Cases org, id, and orgfr assumed gas-particle partitioning into the organic aerosol only. In this case, the role of the seed aerosol is restricted to providing a substrate for nucleation of organic vapours. This is the case for effloresced seed particles. For liquid seed aerosols this is equivalent to a complete organic/electrolyte phase separation with no partitioning of inorganic ions to the organic phase. For cases sd and sdfr equilibrium partitioning between the gas phase and the entire condensed phase including the seed aerosol is assumed, leading in most cases to LLPS. The current model does not yet contain interaction parameters of bisulfate with all involved organic functional groups. Therefore, ammonium bisulfate was treated as ammonium sulfate in the model, and we are not capable of distinguishing whether the enhanced partitioning of semi-volatile vapours in the acidic medium is attributable to additional reactions in the bulk phase (catalysed at lower pH) or to an enhanced solubility of SOA species.

Considering the size-resolved particle chemical composition discussed in Sect. 3.3 (Fig. 4), LLPS is likely not realized within single particles, but the aerosol population splits up into a predominantly organic mode at $\sim$ 200 nm and a predominantly inorganic mode at $\sim$ 400 nm. The formation of these two populations may occur by the homogeneous or heterogeneous nucleation of highly oxidized non-volatile products. Homogeneous nucleation implies new particle formation (which would only be moderate – see Figs. S13 and S14 – due to the high condensation sink in the chamber), while heterogeneous nucleation proceeds via condensational growth (which would occur on smaller particles with a higher surface). Both processes are expected to create small organic-rich particles, providing an organic absorptive phase into which additional semi-volatile compounds may preferentially partition. When the organic and electrolyte phases are present in different particles, the two phases communicate via gas-phase diffusion, and equilibration timescales depend on the components' volatility. For compounds with $C^* = 0.1$–$100\,\mu g\,m^{-3}$, equilibration occurs within timescales of minutes to tens of minutes, assuming no bulk-phase diffusion limitations (Marcolli et al., 2004). In the larger particle electrolyte-rich mode, the inorganic ions would exert a salting-out effect driving the organic compounds to partition to the gas phase or into the smaller organic-rich particles. This would prevent the organic compounds from partitioning in significant amounts into the seed aerosol from the beginning and depleting even further these larger particles from the organic material. Under such a scenario an externally mixed phase-separated aerosol may evolve in the smog chamber. Overall, the size-resolved chemical composition information confirms the modelling results, providing compelling evidence for organic/electrolyte LLPS.

The scenario outlined above is based on equilibrium partitioning and does not invoke diffusion limitations within the condensed phase. Recent evidence may challenge this assumption, suggesting that SOA may adopt a highly viscous state (e.g. Virtanen et al., 2010; Koop et al., 2011), where bulk diffusion and evaporation are kinetically limited. However, while such behaviour occurs under certain conditions, e.g. low temperature and low relative humidity, we expect that this is not the case for the aerosol investigated in this study. Saleh et al. (2013) showed that SOA from α-pinene ozonolysis reaches equilibrium with the gas phase within tens of minutes at low mass loadings (2–12 $\mu g\,m^{-3}$) upon a step change in temperature. Robinson et al. (2013) determined by aerosol mixing experiments that the diffusion coefficient in α-pinene-derived SOA is high enough for mixing on a timescale of minutes. Fast mixing is further supported by measurements of ambient OA (Yatavelli et al., 2014) showing that biogenic SOA reaches equilibrium within atmospheric timescales, under similar conditions to those in our chamber. Therefore, we expect that, if thermodynamically favourable, liquid–liquid mixing would have occurred under the timescales of our experiments and a unimodal particle population would have emerged. However, consistent with model predictions, this is not the case.

5 Summary and conclusions

We conducted a series of smog chamber experiments to investigate the impact of NO_x / VOC ratios, RH and the seed aerosol composition on the yield and the degree of oxygenation of SOA produced from α-pinene photo-oxidation. We developed a novel approach based on Monte Carlo simulations to determine SOA volatility distributions from the measured yields using the volatility basis set framework. Measured yields spanned an order of magnitude (2–20 %), depending on the prevailing oxidation conditions, the particle bulk-phase composition and the water content. This underlines the need to consider these conditions for an accurate prediction of the SOA burden in the atmosphere. The yields increased dramatically with RH, aerosol acidity and at low NO_x. The aerosol bulk chemical composition measured by the HR-ToF-AMS appears to be mostly dependent on NO_x / VOC ratios.

We investigated whether equilibrium partitioning between the gas and condensed phase(s) can reproduce the measured SOA yield and O : C ratio at low and high RH. For this, the AIOMFAC thermodynamic group-contribution model was used to examine the partitioning of a range of selected surrogate compounds with different volatilities and O : C ratios as a function of their activity coefficients and the particle water content, properties that are altered with the variation of RH. In practice, two to four surrogate compounds were assigned to each volatility bin based on the volatility distributions derived from experimental data and the compounds' effective saturation concentration, which depends on the pure component saturation vapour pressures. The RH was then varied in the model and changes in SOA mass and O : C ratios were monitored. There are large discrepancies between vapour pressures determined for semi-volatile and low-volatility compounds, depending on the measurement techniques (Huisman et al., 2013; Bilde et al., 2015), which introduce inaccuracies in saturation vapour pressure estimations. However, these uncertainties do not affect the approach applied in this study because an incorrect assignment of a model compound to a volatility bin does not change the experimentally derived volatility bin distribution. The share of the individual model compounds to the volatility bins was used as a fitting parameter to achieve agreement between measurements and calculations. In addition, as a set of volatility distribution functions was obtained for each experiment through the Monte Carlo simulations, the approach has proven very effective in assessing the sensitivity of equilibrium partitioning calculations to the volatility distribution input parameters.

Our results show that only with the inclusion of fragmentation products could the model simultaneously explain SOA concentrations and O : C ratios. Under these conditions, the model predicts that an increase in RH from $\sim$ 25 to $\sim$ 60 % may lead to a 3-fold enhancement in SOA mass, due to the increase in the absorptive mass and the slight decrease in the compounds' activity coefficients. While the magnitude of this increase is consistent with the experimental observation at low NO_x, equilibrium partitioning alone could not explain the strong increase in the yields with RH observed for the high NO_x experiments (factor $\sim$ 6). This suggests that other processes, including the reactive uptake of semi-volatile species into the liquid phase, may occur and be enhanced at higher RH, especially for compounds formed under high NO_x conditions such as carbonyls. Future studies should investigate the dependence of SOA compounds on RH, NO_x and aerosol acidity at a molecular level. Such measurements shall provide additional insights into the chemical nature of the compounds that additionally partition or react at higher RH and also the mechanisms via which such processes occur.

For most of the cases studied, the model predicts liquid–liquid phase separation into an organic and an electrolyte phase. Considering the size-resolved particle chemical composition, this phase separation is likely not realized within single particles, but the aerosol population splits up into a predominantly organic mode at $\sim$ 200 nm and a predominantly inorganic mode at $\sim$ 400 nm. Based on our results, such liquid–liquid phase separation is expected to occur under most ambient conditions, i.e. similar levels of OA and sulfate, O : C < 0.8, and RH < 70–80 %.

Data availability. The largest part of data related to this article, including experimental conditions, observed yields, O : C ratios

and detailed model outputs, can be found in the tables of this paper and is available online in the Supplement. To access additional data please send a request to imad.el-haddad@psi.ch or urs.Baltensperger@psi.ch.

The Supplement related to this article is available online at doi:10.5194/acp-17-5035-2017-supplement.

Competing interests. The authors declare that they have no conflict of interest.

Acknowledgements. This work has been supported by EU 7th Framework projects EUROCHAMP-2 and PEGASOS, as well as the Swiss National Science Foundation (Ambizione PZ00P2_131673, SAPMAV 200021_13016), the EU commission (FP7, COFUND: PSI-Fellow, grant agreement no. 290605) and CCES-CCEM joint project OPTIWARES. We thank René Richter and Günther Wehrle for their technical support at the smog chamber, and in addition Michel J. Rossi, Martin Gysel, Neil Donahue and Barbara Turpin for the helpful discussions. We thank Andreas Zuend for providing the Fortran code for phase partitioning calculations and AIOMFAC and helpful discussions. We thank the Institute of Meteorology and Climate Research, Karlsruhe Institute of Technology, Germany for providing their HR-ToF-AMS for our measurements.

Edited by: V. Faye McNeill
Reviewed by: two anonymous referees

References

Aiken, A. C., DeCarlo, P. F., and Jimenez, J. L.: Elemental analysis of organic species with electron ionization high-resolution mass spectrometry, Anal. Chem., 79, 8350–8358, 2007.

Aiken, A. C., DeCarlo, P. F., Kroll, J. H., Worsnop, D. R., Huffman, J. A., Docherty, K. S., Ulbrich, I. M., Mohr, C., Kimmel, J. R., Sueper, D., Sun, Y., Zhang, Q., Trimborn, A., Northway, M., Ziemann, P. J., Canagaratna, M. R., Onasch, T. B., Alfarra, M. R., Prevot, A. S. H., Dommen, J., Duplissy, J., Metzger, A., Baltensperger, U., and Jimenez, J. L.: O / C and OM / OC ratios of primary, secondary, and ambient organic aerosols with high-resolution time-of-flight aerosol mass spectrometry, Environ. Sci. Technol., 42, 4478–4485, 2008.

Atkinson, R.: Atmospheric chemistry of VOCs and NO_x, Atmos. Environ., 34, 2063–2101, 2000.

Atkinson, R. and Arey, J.: Gas-phase tropospheric chemistry of biogenic volatile organic compounds: a review, Atmos. Environ., 37, 197–219, doi:10.1016/S1352-2310(03)00391-1, 2003.

Barmet, P., Dommen, J., DeCarlo, P. F., Tritscher, T., Praplan, A. P., Platt, S. M., Prevot, A. S. H., Donahue, N. M., and Baltensperger, U.: OH clock determination by proton transfer reaction mass spectrometry at an environmental chamber, Atmos. Meas. Tech., 5, 647–656, doi:10.5194/amt-5-647-2012, 2012.

Bilde, M., Barsanti, K., Booth, M., Cappa, C. D., Donahue, N. M., Emanuelsson, E. U., McFiggans, G., Krieger, U. K., Marcolli, C., Topping, D., Ziemann, P., Barley, M., Clegg, S., Dennis-Smither, B., Hallquist, M., Hallquist, Å. M., Khlystov, A., Kulmala, M., Mogensen, D., Percival, C. J., Pope, F., Reid, J. P., Ribeiro da Silva, M. A. V., Rosenoern, T., Salo, K., Soonsin, V. P., Yli-Juuti, T., Prisle, N. L., Pagels, J., Rarey, J., Zardini, A. A., and Riipinen, I.: Saturation vapor pressures and transition enthalpies of low-volatility organic molecules of atmospheric relevance: From dicarboxylic acids to complex mixtures, Chem. Rev., 115, 4115–4156, doi:10.1021/cr5005502, 2015.

Bonn, B., Schuster, G., and Moortgat, G. K.: Influence of water vapor on the process of new particle formation during monoterpene ozonolysis, J. Phys. Chem. A, 106, 2869–2881, 2002.

Bozzetti, C., Sosedova, Y., Xiao, M., Daellenbach, K. R., Ulevicius, V., Dudoitis, V., Mordas, G., Byčenkienė, S., Plauškaitė, K., Vlachou, A., Golly, B., Chazeau, B., Besombes, J. L., Baltensperger, U., Jaffrezo, J. L., Slowik, J. G., El Haddad, I., and Prévôt, A. S. H.: Argon offline-AMS source apportionment of organic aerosol over yearly cycles for an urban, rural, and marine site in northern Europe, Atmos. Chem. Phys., 17, 117–141, doi:10.5194/acp-17-117-2017, 2017.

Canagaratna, M. R., Jayne, J. T., Jimenez, J. L., Allan, J. D., Alfarra, M. R., Zhang, Q., Onasch, T. B., Drewnick, F., Coe, H., Middlebrook, A., Delia, A., Williams, L. R., Trimborn, A. M., Northway, M. J., DeCarlo, P. F., Kolb, C. E., Davidovits, P., and Worsnop, D. R.: Chemical and microphysical characterization of ambient aerosols with the Aerodyne aerosol mass spectrometer, Mass Spectrom. Rev., 26, 185–222, 2007.

Canagaratna, M. R., Jimenez, J. L., Kroll, J. H., Chen, Q., Kessler, S. H., Massoli, P., Hildebrandt Ruiz, L., Fortner, E., Williams, L. R., Wilson, K. R., Surratt, J. D., Donahue, N. M., Jayne, J. T., and Worsnop, D. R.: Elemental ratio measurements of organic compounds using aerosol mass spectrometry: characterization, improved calibration, and implications, Atmos. Chem. Phys., 15, 253–272, doi:10.5194/acp-15-253-2015, 2015.

Chang, R. Y. W., Slowik, J. G., Shantz, N. C., Vlasenko, A., Liggio, J., Sjostedt, S. J., Leaitch, W. R., and Abbatt, J. P. D.: The hygroscopicity parameter (κ) of ambient organic aerosol at a field site subject to biogenic and anthropogenic influences: relationship to degree of aerosol oxidation, Atmos. Chem. Phys., 10, 5047–5064, doi:10.5194/acp-10-5047-2010, 2010.

Chhabra, P. S., Lambe, A. T., Canagaratna, M. R., Stark, H., Jayne, J. T., Onasch, T. B., Davidovits, P., Kimmel, J. R., and Worsnop, D. R.: Application of high-resolution time-of-flight chemical ionization mass spectrometry measurements to estimate volatility distributions of α-pinene and naphthalene oxidation products, Atmos. Meas. Tech., 8, 1–18, doi:10.5194/amt-8-1-2015, 2015.

Ciobanu, V. G., Marcolli, C., Krieger, U. K., Zuend, A., and Peter, T.: Efflorescence of ammonium sulfate and coated ammonium sulfate particles: Evidence for surface nucleation, J. Phys. Chem. A, 114, 9486–9495, doi:10.1021/jp103541w, 2010.

Clegg, S. L., Kleeman, M. J., Griffin, R. J., and Seinfeld, J. H.: Effects of uncertainties in the thermodynamic properties of aerosol components in an air quality model – Part 2: Predictions of the vapour pressures of organic compounds, Atmos. Chem. Phys., 8, 1087–1103, doi:10.5194/acp-8-1087-2008, 2008a.

Clegg, S. L., Kleeman, M. J., Griffin, R. J., and Seinfeld, J. H.: Effects of uncertainties in the thermodynamic properties of aerosol components in an air quality model – Part 1: Treatment of inorganic electrolytes and organic compounds in the condensed

phase, Atmos. Chem. Phys., 8, 1057–1085, doi:10.5194/acp-8-1057-2008, 2008b.

Cocker, D. R. I., Clegg, S. L., Flagan, R. C., and Seinfeld, J. H.: The effect of water on gas–particle partitioning of secondary organic aerosol, Part I: α-pinene/ozone system, Atmos. Environ., 35, 6049–6072, 2001.

Compernolle, S., Ceulemans, K., and Müller, J. F.: EVAPORATION: a new vapour pressure estimation methodfor organic molecules including non-additivity and intramolecular interactions, Atmos. Chem. Phys., 11, 9431–9450, doi:10.5194/acp-11-9431-2011, 2011.

DeCarlo, P. F., Kimmel, J. R., Trimborn, A., Northway, M. J., Jayne, J. T., Aiken, A. C., Gonin, M., Fuhrer, K., Horvath, T., Docherty, K. S., Worsnop, D. R., and Jimenez, J. L.: Field-deployable, high-resolution, time-of-flight aerosol mass spectrometer, Anal. Chem., 78, 8281–8289, 2006.

Donahue, N. M., Robinson, A. L., Stanier, C. O., and Pandis, S. N.: Coupled partitioning, dilution, and chemical aging of semivolatile organics, Environ. Sci. Technol., 40, 2635–2643, 2006.

Donahue, N. M., Epstein, S. A., Pandis, S. N., and Robinson, A. L.: A two-dimensional volatility basis set: 1. organic-aerosol mixing thermodynamics, Atmos. Chem. Phys., 11, 3303–3318, doi:10.5194/acp-11-3303-2011, 2011.

Donahue, N. M., Henry, K. M., Mentel, T. F., Kiendler-Scharr, A., Spindler, C., Bohn, B., Brauers, T., Dorn, H. P., Fuchs, H., Tillmann, R., Wahner, A., Saathoff, H., Naumann, K.-H., Möhler, O., Leisner, T., Müller, L., Reinnig, M.-C., Hoffmann, T., Salo, K., Hallquist, M., Frosch, M., Bilde, M., Tritscher, T., Barmet, P., Praplan, A. P., DeCarlo, P. F., Dommen, J., Prévôt, A. S. H., and Baltensperger, U.: Aging of biogenic secondary organic aerosol via gas-phase OH radical reactions, P. Natl. Acad. Sci. USA, 109, 13503–13508, doi:10.1073/pnas.1115186109, 2012a.

Donahue, N. M., Kroll, J. H., Pandis, S. N., and Robinson, A. L.: A two-dimensional volatility basis set – Part 2: Diagnostics of organic-aerosol evolution, Atmos. Chem. Phys., 12, 615–634, doi:10.5194/acp-12-615-2012, 2012b.

Eddingsaas, N. C., Loza, C. L., Yee, L. D., Chan, M., Schilling, K. A., Chhabra, P. S., Seinfeld, J. H., and Wennberg, P. O.: α-pinene photooxidation under controlled chemical conditions – Part 2: SOA yield and composition in low- and high-NO_x environments, Atmos. Chem. Phys., 12, 7413–7427, doi:10.5194/acp-12-7413-2012, 2012.

El Haddad, I., D'Anna, B., Temime-Roussel, B., Nicolas, M., Boreave, A., Favez, O., Voisin, D., Sciare, J., George, C., Jaffrezo, J. L., Wortham, H., and Marchand, N.: Towards a better understanding of the origins, chemical composition and aging of oxygenated organic aerosols: case study of a Mediterranean industrialized environment, Marseille, Atmos. Chem. Phys., 13, 7875–7894, doi:10.5194/acp-13-7875-2013, 2013.

Farmer, D., Matsunaga, A., Docherty, K., Surratt, J., Seinfeld, J., Ziemann, P., and Jimenez, J.: Response of an aerosol mass spectrometer to organonitrates and organosulfates and implications for atmospheric chemistry, P. Natl. Acad. Sci. USA, 107, 6670–6675, 2010.

Hildebrandt, L., Henry, K. M., Kroll, J. H., Worsnop, D. R., Pandis, S. N., and Donahue, N. M.: Evaluating the mixing of organic aerosol components using high-resolution aerosol mass spectrometry, Environ. Sci. Technol., 45, 6329–6335, 2011.

Hoyle, C. R., Boy, M., Donahue, N. M., Fry, J. L., Glasius, M., Guenther, A., Hallar, A. G., Huff Hartz, K., Petters, M. D., Petäjä, T., Rosenoern, T., and Sullivan, A. P.: A review of the anthropogenic influence on biogenic secondary organic aerosol, Atmos. Chem. Phys., 11, 321–343, doi:10.5194/acp-11-321-2011, 2011.

Huisman, A. J., Krieger, U. K., Zuend, A., Marcolli, C., and Peter, T.: Vapor pressures of substituted polycarboxylic acids are much lower than previously reported, Atmos. Chem. Phys., 13, 6647–6662, doi:10.5194/acp-13-6647-2013, 2013.

Iinuma, Y., Müller, C., Böge, O., Gnauk, T., and Herrmann, H.: The formation of organic sulfate esters in the limonene ozonolysis secondary organic aerosol (SOA) under acidic conditions, Atmos. Environ., 41, 5571–5583, 2007.

Jang, M., Czoschke, N. M., Lee, S., and Kamens, R. M.: Heterogeneous atmospheric aerosol production by acid-catalyzed particle-phase reactions, Science, 298, 814–817, 2002.

Jaoui, M. and Kamens, R. M.: Mass balance of gaseous and particulate products analysis from α-pinene/NOx/air in the presence of natural sunlight, J. Geophys. Res., 106, 12541–12558, doi:10.1029/2001JD900005, 2001.

Jimenez, J. L., Canagaratna, M. R., Donahue, N. M., Prevot, A. S. H., Zhang, Q., Kroll, J. H., DeCarlo, P. F., Allan, J. D., Coe, H., Ng, N. L., Aiken, A. C., Docherty, K. S., Ulbrich, I. M., Grieshop, A. P., Robinson, A. L., Duplissy, J., Smith, J. D., Wilson, K. R., Lanz, V. A., Hueglin, C., Sun, Y. L., Tian, J., Laaksonen, A., Raatikainen, T., Rautiainen, J., Vaattovaara, P., Ehn, M., Kulmala, M., Tomlinson, J. M., Collins, D. R., Cubison, M. J. E., Dunlea, J., Huffman, J. A., Onasch, T. B., Alfarra, M. R., Williams, P. I., Bower, K., Kondo, Y., Schneider, J., Drewnick, F., Borrmann, S., Weimer, S., Demerjian, K., Salcedo, D., Cottrell, L., Griffin, R., Takami, A., Miyoshi, T., Hatakeyama, S., Shimono, A., Sun, J. Y., Zhang, Y. M., Dzepina, K., Kimmel, J. R., Sueper, D., Jayne, J. T., Herndon, S. C., Trimborn, A. M., Williams, L. R., Wood, E. C., Middlebrook, A. M., Kolb, C. E., Baltensperger, U., and Worsnop, D. R.: Evolution of organic aerosols in the atmosphere, Science, 326, 1525–1529, doi:10.1126/science.1180353, 2009.

Jonsson, Å. M., Hallquist, M., and Ljungström, E.: Impact of humidity on the ozone initiated oxidation of limonene, Δ3-carene, and α-pinene, Environ. Sci. Technol., 40, 188–194, doi:10.1021/es051163w, 2006.

Kleindienst, T. E., Edney, E. O., Lewandowski, M., Offenberg, J. H., and Jaoui, M.: Secondary organic carbon and aerosol yields from the irradiations of isoprene and α-pinene in the presence of NO_x and SO_2, Environ. Sci. Technol., 40, 3807–3812, 2006.

Kleindienst, T. E., Jaoui, M., Lewandowski, M., Offenberg, J. H., Lewis, C. W., Bhave, P. V., and Edney, E. O.: Estimates of the contributions of biogenic and anthropogenic hydrocarbons to secondary organic aerosol at a southeastern US location, Atmos. Environ., 41, 8288–8300, doi:10.1016/j.atmosenv.2007.06.045, 2007.

Koop, T., Bookhold, J., Shiraiwa, M., and Pöschl, U.: Glass transition and phase state of organic compounds: dependency on molecular properties and implications for secondary organic aerosols in the atmosphere, Phys. Chem. Chem. Phys., 13, 19238–19255, 2011.

Krapf, M., El Haddad, I., Bruns, E., A., Molteni, U., Daellenbach, K. R., Prévôt, A. S. H., Baltensperger, U., and Dommen, J.: La-

bile peroxides in secondary organic aerosol, Chem, 1, 603–616, doi:10.1016/j.chempr.2016.09.007, 2016.

Krechmer, J. E., Pagonis, D., Ziemann, P. J., and Jimenez, J. L.: Quantification of gas-wall partitioning in teflon environmental chambers using rapid bursts of low-volatility oxidized species generated in situ, Environ. Sci. Technol., 50, 5757–5765, doi:10.1021/acs.est.6b00606, 2016.

Kreidenweis, S. M., Koehler, K., DeMott, P. J., Prenni, A. J., Carrico, C., and Ervens, B.: Water activity and activation diameters from hygroscopicity data – Part I: Theory and application to inorganic salts, Atmos. Chem. Phys., 5, 1357–1370, doi:10.5194/acp-5-1357-2005, 2005.

Kroll, J. H. and Seinfeld, J. H.: Chemistry of secondary organic aerosol: Formation and evolution of low-volatility organics in the atmosphere, Atmos. Environ., 42, 3593–3624, 2008.

Li, Y., Pöschl, U., and Shiraiwa, M.: Molecular corridors and parameterizations of volatility in the chemical evolution of organic aerosols, Atmos. Chem. Phys., 16, 3327–3344, doi:10.5194/acp-16-3327-2016, 2016.

Loza, C. L., Chan, A. W. H., Galloway, M. M., Keutsch, F. N., Flagan, R. C., and Seinfeld, J. H.: Characterization of vapor wall loss in laboratory chambers, Environ. Sci. Technol., 44, 5074–5078, doi:10.1021/es100727v, 2010.

Marcolli, C. and Krieger, U. K.: Phase changes during hygroscopic cycles of mixed organic/inorganic model systems of tropospheric aerosols, J. Phys. Chem. A, 110, 1881–1893, doi:10.1021/jp0556759, 2006.

Marcolli, C., Luo, B. P., Peter, Th., and Wienhold, F. G.: Internal mixing of the organic aerosol by gas phase diffusion of semivolatile organic compounds, Atmos. Chem. Phys., 4, 2593–2599, doi:10.5194/acp-4-2593-2004, 2004.

Martin, S. T.: Phase transitions of aqueous atmospheric particles, Chem. Rev., 100, 3403–3454, 2000.

Massoli, P., Lambe, A. T., Ahern, A. T., Williams, L. R., Ehn, M., Mikkilä, J., Canagaratna, M. R., Brune, W. H., Onasch, T. B., Jayne, J. T., Petäjä, T., Kulmala, M., Laaksonen, A., Kolb, C. E., Davidovits, P., and Worsnop, D. R.: Relationship between aerosol oxidation level and hygroscopic properties of laboratory generated secondary organic aerosol (SOA) particles, Geophys. Res. Lett., 37, L24801, doi:10.1029/2010GL045258, 2010.

Mutzel, A., Poulain, L., Berndt, T., Iinuma, Y., Rodigast, M., Böge, O., Richters, S., Spindler, G., Sipilä, M., Jokinen, T., Kulmala, M., and Herrmann, H.: Highly oxidized multifunctional organic compounds observed in tropospheric particles: a field and laboratory study, Environ. Sci. Technol., 49, 7754–7761, doi:10.1021/acs.est.5b00885, 2015.

Nah, T., McVay, R. C., Zhang, X., Boyd, C. M., Seinfeld, J. H., and Ng, N. L.: Influence of seed aerosol surface area and oxidation rate on vapor wall deposition and SOA mass yields: a case study with α-pinene ozonolysis, Atmos. Chem. Phys., 16, 9361–9379, doi:10.5194/acp-16-9361-2016, 2016.

Ng, N. L., Chhabra, P. S., Chan, A. W. H., Surratt, J. D., Kroll, J. H., Kwan, A. J., McCabe, D. C., Wennberg, P. O., Sorooshian, A., Murphy, S. M., Dalleska, N. F., Flagan, R. C., and Seinfeld, J. H.: Effect of NOx level on secondary organic aerosol (SOA) formation from the photooxidation of terpenes, Atmos. Chem. Phys., 7, 5159–5174, doi:10.5194/acp-7-5159-2007, 2007.

Ng, N. L., Canagaratna, M. R., Jimenez, J. L., Chhabra, P. S., Seinfeld, J. H., and Worsnop, D. R.: Changes in organic aerosol composition with aging inferred from aerosol mass spectra, Atmos. Chem. Phys., 11, 6465–6474, doi:10.5194/acp-11-6465-2011, 2011a.

Nguyen, T. B., Tyndall, G. S., Crounse, J. D., Teng, A. P., Bates, K. H., Schwantes, R. H., Coggon, M. M., Zhang, L., Feiner, P., and Milller, D. O.: Atmospheric fates of Criegee intermediates in the ozonolysis of isoprene, Phys. Chem. Chem. Phys., 18, 10241–10254, 2016.

Odum, J. R., Hoffmann, T., Bowman, F., Collins, D., Flagan, R. C., and Seinfeld, J. H.: Gas/particle partitioning and secondary organic aerosol yields, Environ. Sci. Technol., 30, 2580–2585, doi:10.1021/es950943+, 1996.

Pankow, J. F.: An absorption model of the gas/aerosol partitioning involved in the formation of secondary organic aerosol, Atmos. Environ., 28, 189–193, 1994.

Pankow, J. F.: Organic particulate material levels in the atmosphere: Conditions favoring sensitivity to varying relative humidity and temperature, P. Natl. Acad. Sci. USA, 107, 6682–6686, doi:10.1073/pnas.1001043107, 2010.

Paulsen, D., Dommen, J., Kalberer, M., Prévôt, A. S. H., Richter, R., Sax, M., Steinbacher, M., Weingartner, E., and Baltensperger, U.: Secondary organic aerosol formation by irradiation of 1,3,5-trimethylbenzene-NO_x-H_2O in a new reaction chamber for atmospheric chemistry and physics, Environ. Sci. Technol., 39, 2668–2678, 2005.

Pfaffenberger, L., Barmet, P., Slowik, J. G., Praplan, A. P., Dommen, J., Prévôt, A. S. H., and Baltensperger, U.: The link between organic aerosol mass loading and degree of oxygenation: An α-pinene photooxidation study, Atmos. Chem. Phys., 13, 6493–6506, doi:10.5194/acp-13-6493-2013, 2013.

Pieber, S. M., El Haddad, I., Slowik, J. G., Canagaratna, M. R., Jayne, J. T., Platt, S. M., Bozzetti, C., Daellenbach, K. R., Fröhlich, R., Vlachou, A., Klein, F., Dommen, J., Miljevic, B., Jiménez, J. L., Worsnop, D. R., Baltensperger, U., and Prévôt, A. S. H.: Inorganic salt interference on CO_2^+ in Aerodyne AMS and ACSM organic aerosol composition studies, Environ. Sci. Technol., 50, 10494–10503, doi:10.1021/acs.est.6b01035, 2016.

Platt, S. M., El Haddad, I., Zardini, A. A., Clairotte, M., Astorga, C., Wolf, R., Slowik, J. G., Temime-Roussel, B., Marchand, N., Ježek, I., Drinovec, L., Močnik, G., Möhler, O., Richter, R., Barmet, P., Bianchi, F., Baltensperger, U., and Prévôt, A. S. H.: Secondary organic aerosol formation from gasoline vehicle emissions in a new mobile environmental reaction chamber, Atmos. Chem. Phys., 13, 9141–9158, doi:10.5194/acp-13-9141-2013, 2013.

Platt, S. M., Haddad, I. E., Pieber, S. M., Huang, R. J., Zardini, A. A., Clairotte, M., Suarez-Bertoa, R., Barmet, P., Pfaffenberger, L., Wolf, R., Slowik, J. G., Fuller, S. J., Kalberer, M., Chirico, R., Dommen, J., Astorga, C., Zimmermann, R., Marchand, N., Hellebust, S., Temime-Roussel, B., Baltensperger, U., and Prévôt, A. S. H.: Two-stroke scooters are a dominant source of air pollution in many cities, Nat. Commun., 5, 3749, doi:10.1038/ncomms4749, 2014.

Presto, A. A., Huff Hartz, K. E., and Donahue, N. M.: Secondary organic aerosol production from terpene ozonolysis, 2. Effect of NO_x concentration, Environ. Sci. Technol., 39, 7046–7054, doi:10.1021/es050400s, 2005.

Prisle, N. L., Engelhart, G. J., Bilde, M., and Donahue, N. M.: Humidity influence on gas-particle phase partitioning of α-

pinene + O_3 secondary organic aerosol, Geophys. Res. Lett., 37, L01802, doi:10.1029/2009GL041402, 2010.

Robinson, E. S., Saleh, R., and Donahue, N. M.: Organic aerosol mixing observed by single-particle mass spectrometry, J. Phys. Chem., 117, 13935–13945, doi:10.1021/jp405789t, 2013.

Saleh, R., Donahue, N. M., and Robinson, A. L.: Time scales for gas-particle partitioning equilibration of secondary organic aerosol formed from alpha-pinene ozonolysis, Environ. Sci. Technol., 47, 5588–5594, doi:10.1021/es400078d, 2013.

Shiraiwa, M., Yee, L. D., Schilling, K. A., Loza, C. L., Craven, J. S., Zuend, A., Ziemann, P. J., and Seinfeld, J. H.: Size distribution dynamics reveal particle-phase chemistry in organic aerosol formation, P. Natl. Acad. Sci. USA, 110, 11746–11750, doi:10.1073/pnas.1307501110, 2013.

Song, M., Marcolli, C., Krieger, U. K., Zuend, A., and Peter, T.: Liquid-liquid phase separation and morphology of internally mixed dicarboxylic acids/ammonium sulfate/water particles, Atmos. Chem. Phys., 12, 2691–2712, doi:10.5194/acp-12-2691-2012, 2012.

Stokes, R. and Robinson, R.: Interactions in aqueous nonelectrolyte solutions, I. Solute-solvent equilibria, J. Phys. Chem., 70, 2126–2131, 1966.

Taira, M. and Kanda, Y.: Continuous generation system for low-concentration gaseous nitrous acid, Anal. Chem., 62, 630–633, 1990.

Topping, D. O., McFiggans, G. B., and Coe, H.: A curved multi-component aerosol hygroscopicity model framework: Part 1 – Inorganic compounds, Atmos. Chem. Phys., 5, 1205–1222, doi:10.5194/acp-5-1205-2005, 2005.

Tröstl, J., Chuang, W. K., Gordon, H., Heinritzi, M., Yan, C., Molteni, U., Ahlm, L., Frege, C., Bianchi, F., Wagner, R., Simon, M., Lehtipalo, K., Williamson, C., Craven, J. S., Duplissy, J., Adamov, A., Almeida, J., Bernhammer, A.-K., Breitenlechner, M., Brilke, S., Dias, A., Ehrhart, S., Flagan, R. C., Franchin, A., Fuchs, C., Guida, R., Gysel, M., Hansel, A., Hoyle, C. R., Jokinen, T., Junninen, H., Kangasluoma, J., Keskinen, H., Kim, J., Krapf, M., Kürten, A., Laaksonen, A., Lawler, M., Leiminger, M., Mathot, S., Möhler, O., Nieminen, T., Onnela, A., Petäjä, T., Piel, F. M., Miettinen, P., Rissanen, M. P., Rondo, L., Sarnela, N., Schobesberger, S., Sengupta, K., Sipilä, M., Smith, J. N., Steiner, G., Tomè, A., Virtanen, A., Wagner, A. C., Weingartner, E., Wimmer, D., Winkler, P. M., Ye, P., Carslaw, K. S., Curtius, J., Dommen, J., Kirkby, J., Kulmala, M., Riipinen, I., Worsnop, D. R., Donahue, N. M., and Baltensperger, U.: The role of low-volatility organic compounds in initial particle growth in the atmosphere, Nature, 533, 527–531, 2016

Valorso, R., Aumont, B., Camredon, M., Raventos-Duran, T., Mouchel-Vallon, C., Ng, N. L., Seinfeld, J. H., Lee-Taylor, J., and Madronich, S.: Explicit modelling of SOA formation from α-pinene photooxidation: sensitivity to vapour pressure estimation, Atmos. Chem. Phys., 11, 6895–6910, doi:10.5194/acp-11-6895-2011, 2011.

Virtanen, A., Joutsensaari, J., Koop, T., Kannosto, J., Yli-Pirila, P., Leskinen, J., Makela, J. M., Holopainen, J. K., Poschl, U., Kulmala, M., Worsnop, D. R., and Laaksonen, A.: An amorphous solid state of biogenic secondary organic aerosol particles, Nature, 467, 824–827, doi:10.1038/nature09455, 2010.

Williams, L. R., Gonzalez, L. A., Peck, J., Trimborn, D., McInnis, J., Farrar, M. R., Moore, K. D., Jayne, J. T., Robinson, W. A., Lewis, D. K., Onasch, T. B., Canagaratna, M. R., Trimborn, A., Timko, M. T., Magoon, G., Deng, R., Tang, D., de la Rosa Blanco, E., Prévôt, A. S. H., Smith, K. A., and Worsnop, D. R.: Characterization of an aerodynamic lens for transmitting particles greater than 1 micrometer in diameter into the Aerodyne aerosol mass spectrometer, Atmos. Meas. Tech., 6, 3271–3280, doi:10.5194/amt-6-3271-2013, 2013.

Yatavelli, R. L. N., Stark, H., Thompson, S. L., Kimmel, J. R., Cubison, M. J., Day, D. A., Campuzano-Jost, P., Palm, B. B., Hodzic, A., Thornton, J. A., Jayne, J. T., Worsnop, D. R., and Jimenez, J. L.: Semicontinuous measurements of gas–particle partitioning of organic acids in a ponderosa pine forest using a MOVI-HRToF-CIMS, Atmos. Chem. Phys., 14, 1527–1546, doi:10.5194/acp-14-1527-2014, 2014.

You, Y., Renbaum-Wolff, L., and Bertram, A. K.: Liquid–liquid phase separation in particles containing organics mixed with ammonium sulfate, ammonium bisulfate, ammonium nitrate or sodium chloride, Atmos. Chem. Phys., 13, 11723–11734, doi:10.5194/acp-13-11723-2013, 2013.

You, Y., Smith, M. L., Song, M., Martin, S. T., and Bertram, A. K.: Liquid–liquid phase separation in atmospherically relevant particles consisting of organic species and inorganic salts, Int. Rev. Phys. Chem., 33, 43–77, doi:10.1080/0144235X.2014.890786, 2014.

Zhang, X., Cappa, C. D., Jathar, S. H., McVay, R. C., Ensberg, J. J., Kleeman, M. J., and Seinfeld, J. H.: Influence of vapor wall loss in laboratory chambers on yields of secondary organic aerosol, P. Natl. Acad. Sci. USA, 111, 5802–5807, doi:10.1073/pnas.1404727111, 2014.

Zhang, X., Schwantes, R. H., McVay, R. C., Lignell, H., Coggon, M. M., Flagan, R. C., and Seinfeld, J. H.: Vapor wall deposition in Teflon chambers, Atmos. Chem. Phys., 15, 4197–4214, doi:10.5194/acp-15-4197-2015, 2015.

Zuend, A. and Seinfeld, J. H.: Modeling the gas-particle partitioning of secondary organic aerosol: the importance of liquid-liquid phase separation, Atmos. Chem. Phys., 12, 3857–3882, doi:10.5194/acp-12-3857-2012, 2012.

Zuend, A. and Seinfeld, J. H.: A practical method for the calculation of liquid–liquid equilibria in multicomponent organic–water–electrolyte systems using physicochemical constraints, Fluid Phase Equilibr., 337, 201–213, doi:10.1016/j.fluid.2012.09.034, 2013.

Zuend, A., Marcolli, C., Luo, B. P., and Peter, T.: A thermodynamic model of mixed organic-inorganic aerosols to predict activity coefficients, Atmos. Chem. Phys., 8, 4559–4593, doi:10.5194/acp-8-4559-2008, 2008.

Zuend, A., Marcolli, C., Peter, T., and Seinfeld, J. H.: Computation of liquid-liquid equilibria and phase stabilities: implications for RH-dependent gas/particle partitioning of organic-inorganic aerosols, Atmos. Chem. Phys., 10, 7795–7820, doi:10.5194/acp-10-7795-2010, 2010.

Zuend, A., Marcolli, C., Booth, A. M., Lienhard, D. M., Soonsin, V., Krieger, U. K., Topping, D. O., McFiggans, G., Peter, T., and Seinfeld, J. H.: New and extended parameterization of the thermodynamic model AIOMFAC: calculation of activity coefficients for organic-inorganic mixtures containing carboxyl, hydroxyl, carbonyl, ether, ester, alkenyl, alkyl, and aromatic functional groups, Atmos. Chem. Phys., 11, 9155–9206, doi:10.5194/acp-11-9155-2011, 2011.